AGU100 ADVANCING EARTH AND SPACE SCIENCE

Geochemistry, Geophysics, Geosystems

RESEARCH ARTICLE
10.1002/2017GC007318

PSV10: A Global Data Set for 0–10 Ma Time-Averaged Field and Paleosecular Variation Studies

G. Cromwell[1], C. L. Johnson[2,3], L. Tauxe[1], C. G. Constable[4], and N. A. Jarboe[1]

[1]Geosciences Research Division, Scripps Institution of Oceanography, University of California San Diego, La Jolla, CA, USA, [2]Department of Earth, Ocean and Atmospheric Sciences, University of British Columbia, Vancouver, BC, Canada, [3]Planetary Science Institute, Tucson, AZ, USA, [4]Institute of Geophysics and Planetary Physics, Scripps Institution of Oceanography, University of California San Diego, La Jolla, CA, USA

Key Points:
- We compiled a new data set, PSV10, that comprises 2,401 selected paleomagnetic directions from lava flows 0–10 Ma in age
- Virtual geomagnetic pole dispersion and inclination anomaly are compared with an existing time-averaged field and paleosecular variation models
- New time-averaged field models built from the 0–5 Ma normal polarity subset of PSV10 show non-zonal structure

Supporting Information:
- Supporting Information S1
- Data Set S1
- Data Set S2
- Data Set S3

Correspondence to:
G. Cromwell,
geoffrey.cromwell@gmail.com,
gcromwell@usgs.gov

Citation:
Cromwell, G., Johnson, C. L., Tauxe, L., Constable, C. G., & Jarboe, N. A. (2018). PSV10: A global data set for 0–10 Ma time-averaged field and paleosecular variation studies. *Geochemistry, Geophysics, Geosystems*, *19*, 1533–1558. https://doi.org/10.1002/2017GC007318

Received 6 NOV 2017
Accepted 9 MAR 2018
Accepted article online 30 MAR 2018
Published online 14 MAY 2018

Abstract Globally distributed paleomagnetic data from discrete volcanic sites have previously been used for statistical studies of paleosecular variation and the structure of the time-averaged field. We present a new data compilation, PSV10, selected from high-quality paleodirections recorded over the past 10 Ma and comprising 2,401 sites from 81 studies. We require the use of modern laboratory and processing methods, a minimum of four samples per site, and within-site Fisher precision parameter, k_w, $\geq$50. Studies that identify significant tectonic effects or explicitly target transitional field states are excluded, thereby reducing oversampling of transitional time intervals. Additionally, we apply two approaches using geological evidence to minimize effects of short-term serial correlation. PSV10 is suitable for use in new global geomagnetic and paleomagnetic studies as it has greatly improved spatial coverage of sites, especially at equatorial and high latitudes. VGP dispersion is latitudinally dependent, with substantially higher values in the Southern Hemisphere than at corresponding northern latitudes when no VGP cutoff is imposed. Average inclination anomalies for 10° latitude bins range from about $+3 \pm 2°$ to $-7.5 \pm 2°$ for the entire data set, with the largest negative values occurring at equatorial and mid-northern latitudes. New 0–5 Ma TAF models (LN3 and LN3-SC) based on selections of normal polarity data from PSV10 indicate a g_2^0 term that is 3.0% of g_1^0. Non-zonal variations in field structure are observed near the magnetic equator and in regions of increased radial flux at high latitudes over the Americas, the Indian Ocean, and Asia.

1. Introduction

Paleomagnetic directional and intensity data have been used since the 1960s to study both the paleosecular variation (PSV) and time-averaged field (TAF) structure of Earth's magnetic field (see Johnson & McFadden, 2015, for a recent review). The focus is usually on discrete time intervals, and several global compilations of paleodirectional data from lava flows emplaced over the last five million years have been used for global and regional TAF and PSV studies (e.g., Johnson & Constable, 1996; Johnson et al., 2008; Lee, 1983; McElhinny & McFadden, 1997; McElhinny & Merrill, 1975; Quidelleur et al., 1994). The overall goals for such studies have been to study the behavior of the geodynamo by documenting both the average departure of geomagnetic field structure from that of a geocentric axial-dipole (GAD) and the typical field variability associated with PSV.

Results derived from lava flows that cooled rapidly in the ambient magnetic field have generally been considered most suitable for PSV studies because, in contrast to the varied levels of smoothing inherent in sedimentary records, the thermal remanent magnetization provides an essentially instantaneous record. However, the uneven global and temporal distribution of accessible volcanic units and limitations in chronological constraints dictate the need to use a statistical approach for TAF and PSV models that span the past few million years. Important questions related to this approach are as follows: (1) how long a time interval is needed to represent any TAF state and its variability? (2) Can the spatial and temporal distributions from multiple globally distributed sites be considered representative of the specific time interval under study? (3) How does the quality of the paleomagnetic record influence the analysis? For example, Ziegler et al. (2011) and Valet et al. (2005) found different average axial-dipole strength for the Brunhes and Matuyama polarity chrons, suggesting different average field behavior over time scales of 1,000 kyr (10^6 years), however, numerical dynamo simulations by Davies and Constable (2014) suggest that a shorter

averaging interval (perhaps 15–20 kyr) may be adequate to resolve the basic morphology (but not necessarily the relative amplitude) of the non-axial-dipole part of the field.

An ideal data set would contain full vector paleomagnetic data with a homogenous global distribution and with each location adequately sampling an interval on the order of 10^6 years (Valet et al., 2005; Ziegler et al., 2011), from perhaps 100–200 sites (Lhuillier & Gilder, 2013), to average out dipole variation of the geomagnetic field. Obtaining such a collection is at present impossible. Nevertheless, the distribution and number of paleomagnetic (directional) sites spanning the past few million years does provide a useful basis for statistical studies of the geomagnetic field. Results can be used to assess whether there is a typical average field state, explore whether there are differences between normal and reverse polarity states, assess the need for non-zonal (longitudinally varying) time-averaged field structure, delineate geographical variations in PSV, and assess the likelihood of observing excursions and reversals.

TAF models are usually based on a low resolution spherical harmonic description of the geomagnetic field (Johnson & Constable, 1995), in which Gauss coefficients (the g_l^m and h_l^m of degree, l, and order, m,) representing departures from GAD are estimated from globally distributed time-averaged field measurements and their uncertainties. Use of directional rather than full vector data means that only values relative to the axial-dipole g_1^0 can be recovered. The largest estimated contributions are predominantly zonal (the axial quadrupole $\bar{g}_2^0$ and octupole $\bar{g}_3^0$ terms) and are typically a few percent of g_1^0 (Johnson & McFadden, 2015). The need for non-zonal TAF contributions, inferred by Johnson and Constable (1995, 1997) and Gubbins and Kelly (1993) from declination and inclination anomalies relative to GAD directions, has been considered controversial (McElhinny et al., 1996; see also Johnson & McFadden, 2015, and references therein). A global data set with improved data quality, temporal and spatial distribution is needed to help resolve this issue.

Once a TAF model is established it is possible to define statistical variability about the expected mean value of the field. Useful diagnostic data for PSV studies are the geographical variation of dispersion in virtual geomagnetic pole (VGP) positions, and numerous PSV models, (labeled Models A through G, see Johnson & McFadden, 2015; Merrill et al., 1996) have been parameterized in terms of expected latitudinal variations in such observations. Giant Gaussian Process (GGP) models (Constable & Parker, 1988) have also been used to provide a statistical representation of the average field and its paleosecular variation through a description of statistical variability in the Gauss coefficients (e.g., CP88 (Constable & Parker, 1988), QC96 (Quidelleur & Courtillot, 1996), CJ98 (Constable & Johnson, 1999), and TK03 (Tauxe & Kent, 2004)). Other models build on the forward modeling approach of GGP studies and provide statistical tests for compatibility of time average field and paleosecular variation field parameters (e.g., Khokhlov & Hulot, 2013). For a review of these different models, see Johnson and McFadden (2015).

We have selected Model G (McElhinny & McFadden, 1997) and TK03 as representatives for comparison with the new data sets to be discussed later; both were based on the paleosecular variation from recent lavas (PSVRL) database (McElhinny & McFadden, 1997). Model G is designed to fit VGP dispersion at different latitudes using the functional form:

$$S=\sqrt{(a\lambda)^2+b^2}, \quad (1)$$

where S is VGP dispersion about GAD, λ is latitude, and a and b are interpreted as contributions from antisymmetric ($l-m$ odd) and symmetric ($l-m$ even) families of Gauss coefficients, respectively. TK03 is a GGP statistical model that predicts full vector distributions of the geomagnetic field at any latitude and longitude. In TK03, the only nonzero TAF contribution is the axial-dipole term, $\bar{g}_1^0$. Two other parameters, α and β, determine the temporal variability. As in Model G, they control the overall level of variation of VGP dispersion and its variation with latitude, through constraints on the relative importance of contributions from Gauss coefficients in the antisymmetric and symmetric families. However, the latitudinal variation in S predicted by TK03 differs from that predicted by Model G because the GPP model explicitly specifies the structure of the spatial power spectrum (Lowes, 1974) at the surface of Earth's core.

Differences in TAF and PSV over time and between normal and reverse polarity chrons are of interest because they could reflect distinct paleomagnetic field

Table 1
*Summary of Demagnetization Codes (DC) (*McElhinny & McFadden, 2000*)*

DC	Description
0	Only Natural remanent magnetization (NRM) values reported.
1	Only NRM values reported. Demagnetization diagrams on pilot specimens indicate stability.
2	Bulk demagnetization at a single step for all specimens. No supporting diagrams.
3	Bulk demagnetization at a single step. Demagnetograms of pilot specimens justify procedure.
4	Principle component analysis (PCA) carried out from analysis of Zijderveld diagrams. One demagnetization method used (Thermal or Alternating Field).
5	PCA analysis derived from Zijderveld diagrams. Two demagnetization methods used.

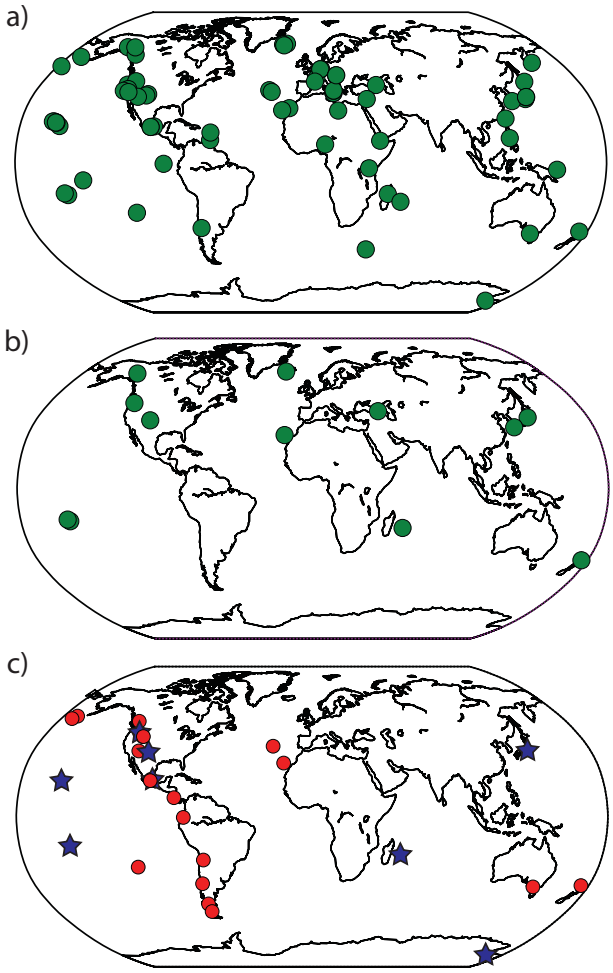

Figure 1. (a) Sampling regions for the PSVRL data base, $N = 3{,}719$ (McElhinny & McFadden, 1997). (b) Locations of sites in PSVRL that are DC-4 (see text), $N = 440$. (c) Locations of sites included in the time-averaged field analysis of Johnson et al. (2008). Red circles are studies performed as part of the Time-Averaged Field Initiative project, all sites are DC-4 or DC-5, $N = 894$. Blue stars are general locations of regional collections containing sites with variable laboratory methods, $N = 1{,}213$.

states. However, careful evaluation of data quality, often represented by demagnetization code (DC, ranges from 0 to 5, see Table 1), and of temporal and spatial sampling distribution plays an important role in the ability to resolve genuine differences. In the PSVRL collection, for which global sampling locations are shown in Figure 1a, McElhinny and McFadden (1997) observed higher VGP dispersion and larger non-axial-dipole contributions to TAF in reversely magnetized rocks than in sites with normal polarities at similar latitudes. Most sites in PSVRL were not thoroughly cleaned, therefore the difference in VGP dispersion and TAF between normal and reverse polarities could be due to bias from residual viscous remanent magnetization in reverse polarity rocks, imparted by the ambient normal polarity field during the Brunhes Chron.

Recent field studies combined with the near universal adoption of modern laboratory methods within the paleomagnetic community have resulted in numerous new, high-quality, paleodirectional sites that span the globe from the Antarctic to the Arctic. It is now worthwhile to re-evaluate PSV and the TAF and address some questions arising from low data quality and poor global distribution. This paper presents a new paleomagnetic compilation, PSV10, that includes all high-quality paleodirectional data from 0 to 10 Ma volcanic units that were published through the end of 2017. In sections 2 and 3, we motivate our selection criteria and describe our new data compilation. Simulations and bootstrap resampling are used to illuminate the effects of sample size, and laboratory methods on overall data quality and on some PSV interpretations. In section 4, we introduce two strategies for mitigating the impact of short-term serial correlation associated with bias in temporal sampling. This analysis is followed in section 5 by a discussion of VGP dispersion and inclination anomalies for the entire PSV10 data set, and for subsets that attempt corrections for serial correlation of sampled lava flows. Special attention is paid to the differences across the various subsets, between normal and reverse polarity data, and how these new data compare to model predictions of Model G and TK03. Finally, in section 6, we select normal polarity subsets of PSV10 that comprise sufficient observations to develop non-zonal, time-averaged field models. We compare these new non-zonal TAF models with previous such models based on 0–5 Ma lava flows, and with results from Holocene field modeling.

2. Establishing Criteria for the PSV10 Data Compilation

Basic criteria for TAF and PSV studies using lava flows have been laid out in numerous publications (see review in Johnson & McFadden, 2015). To date, PSVRL is the most widely used database and contains 3,719 directional sites, drawn from studies of lava flows emplaced in the 0–5 Ma interval that exhibit no evidence of significant tectonic effects since the acquisition of magnetic remanence (Figure 1a). Three further considerations are usually invoked in selecting from these data for PSV and TAF studies:

1. The characteristic remanent direction must be established by laboratory cleaning; undetected magnetic overprints can lead to increased scatter and/or bias in estimates of paleofield directions.
2. An assessment of within-site error is required in the form of a precision estimate, such as α_{95}, or the Fisher precision statistic, k (Fisher, 1953); any estimate of within-site error depends on the number of specimens used, and so each study must specify the number of accepted specimens per site.

3. Sites recording transitional directions are identified and typically removed, so as to only include "typical stable polarity" field estimates. Generally such sites are identified via their VGP latitudes, and sites with low latitude VGPs are removed, e.g., within, say, 45° of the equator, or a cutoff minimum determined by an iterative method (Vandamme, 1994).

Items (1) and (2) are related to data quality and can be studied using defined metrics which we evaluate in section 2.1. The third item is a somewhat subjective decision, as the definition of transitional directions remains ambiguous (e.g., Panovska & Constable, 2017). Also, the limitations of the Vandamme method for evaluating PSV are illuminated in recent work by Suttie et al. (2015).

Only 440 (or ∼12%) of the PSVRL sites are of the highest quality, demagnetization codes (as defined by McElhinny & McFadden, 2000) of DC-4 or DC-5 (Table 1 and Figure 1b) and meet modern laboratory standards for complete demagnetization of all specimens. PSV models TK03 and Model G made no distinction among directional sites of different laboratory quality. The inclusion of lower quality data in these models was deemed necessary at the time because of the limited number of sites. The issues of how many samples per site are needed to establish a reliable site mean direction, and whether the inclusion of samples with no or little demagnetization affects interpretations of paleofield behavior have been active areas of discussion in the literature (e.g., Johnson et al., 2008; Lawrence et al., 2006; Tauxe et al., 2003). We evaluate these two issues in more detail below to establish selection criteria for our data set.

2.1. Modern Data Sets and Bootstrap Simulations From Fisher Distributions

We use bootstrap simulations on real data from a typical modern paleomagnetic study, together with synthetic simulations based on the Fisher distribution, to explore the effects of different numbers of samples per site (n) and incomplete demagnetization on PSV estimates. The circular standard deviation (Fisher, 1953) quantifies the angular variability in direction for both the within-site and between-site dispersion in directions. Within-site circular standard deviation (c_w) is a measure of the precision of a site-level paleodirection, and between-site circular standard deviation (c_s) is a measure of PSV for a collection of sites spanning several hundred kyr. The data set used in our simulations comprises directional results from 37 lavas in Patagonia (published by Mejia et al. (2004) and available from the MagIC database at https://earthref.org/MagIC/DOI/10.1029/2003GC000633) to evaluate site and study-level variabilities. Mejia et al. (2004) was chosen for this analysis because it uses modern laboratory methods (DC-5) with both alternating field and thermal demagnetization, required at least five samples per site, with a minimum within-site Fisher precision statistic of $k_w \geq 50$, has a total number of sites (∼50) typical of many paleodirectional studies, and had specimen-level data available in the MagIC database.

2.1.1. Number of Samples per Site

Our first simulation explores how varying the number of samples per site affects estimates of c_w, hence the precision of the site-level mean direction. Figure 2a shows the estimated site-level c_w for parametric bootstrapped simulations of 1,000 sites with n samples per site. Each set of 1,000 sites is drawn from a Fisher distribution of n samples with precision parameter $\kappa_w = 50$, which is equivalent to a c_w of 11.45°. The variance in c_w depends less strongly on n at approximately $n \geq 4$ or 5, although having twice as many samples ($n = 8$) reduces the total variance of the estimated c_w by an additional 40%. Tauxe et al. (2003) reached a similar conclusion through a simulation on synthetic directions drawn from a distribution with $\kappa_w = 100$. The variance c_w continues to decrease in Figure 2a and appears to level out around $n = 17$. It is clear that having more paleomagnetic samples per site is beneficial, but it is not always practical to collect tens of samples per site during short field seasons. Most published paleomagnetic studies require a minimum n of at least three to five samples per site.

To explore the effect of n on between-site or study-level variance, c_s, estimates from actual paleomagnetic data, we use an empirical bootstrap on the data set from Patagonia by Mejia et al. (2004). We used measurement level data to randomly select n samples from each of the 55 sites, calculated the resulting mean site-level direction for each site, and from that the resulting c_s. This calculation was performed 1,000 times for each n. Dispersion estimates from our simulations rapidly approach the published value of c_s as the number of samples per site increases from three to four, with a more gradual increase in precision when five samples are used. Observations from this simulation on real data suggest that a minimum of four samples per site is necessary to adequately describe the PSV behavior of the magnetic field, at least when using a within-site precision requirement of $k_w \geq 50$.

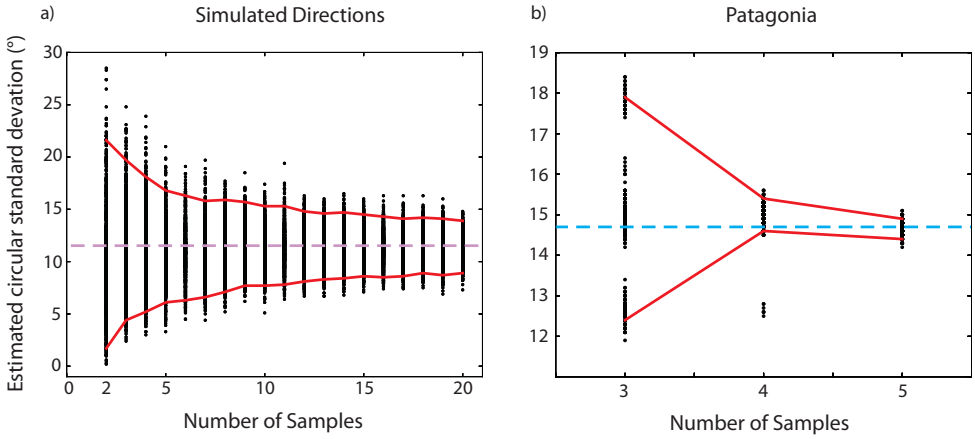

Figure 2. Effects of different numbers of samples per site (n) on within-site (c_w) or between-site (c_s) estimates of circular standard deviation. (a) Estimated site-level c_w for 1,000 sites, each with n samples, drawn from a Fisher distribution with $\kappa_w = 50$ (the equivalent $c_w = 11.45°$, dashed purple line). Ninety-five percent confidence bounds are heavy red lines. (b) Bootstrapped estimates of c_s calculated 1,000 times with different n samples per site for Patagonia (Mejia et al., 2004). Samples for each site are randomly drawn from the published characteristic remanent interpretations. As n increases, the number of sites decreases, resulting in replicate c_s estimates and overlapping dots in Figure 2b. Blue dashed line is the c_s from all published results, red solid lines are 95% confidence bounds.

2.1.2. Quality of Laboratory Demagnetization

Having established a minimum requirement of four samples per site, we examine the hypothesis that unremoved overprints can cause high between-site scatter and anomalous TAF directions. Specifically, we explore whether or not sites demagnetized as DC-2 (each specimen subjected to a blanket demagnetization step) have a greater variance than "high-quality" DC-4 sites (every specimen fully demagnetized and the direction based on principle component analysis). For this analysis we again use the raw measurement and specimen-level data from Mejia et al. (2004). Figure 3a shows cumulative distribution functions of bootstrapped c_s from simulated sites using DC-2 and DC-4 methodologies. In order to maintain

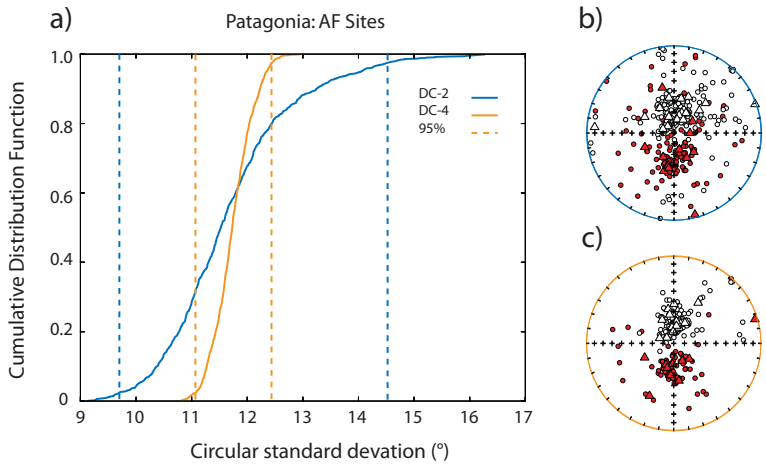

Figure 3. (a) Differences in estimated c_s between simulated DC-2 (blue) and DC-4 (orange) directional sites using the data set from Patagonia (Mejia et al., 2004). Blanket steps of 30 mT were chosen for sites with a minimum of four alternating field samples. Blanket sample directions are randomly selected from the published measurement level data. DC-4 comparisons are drawn from the same samples in the DC-2 sites, except that we randomly select four full vector directions from the published study. Colored dashed lines are 95% confidence bounds. Equal area plots of published samples (circles) and calculated site mean directions (triangles, $n = 4$) are plotted for the (b) DC-2 and (c) DC-4 simulations. Red (white) circles and triangles plot in the lower (upper) hemispheres.

consistency between data selected for each method, we use only specimens cleaned by alternating field (AF) demagnetization. For the DC-2 simulation we randomly select four samples per site and for each of the 55 sites choose the directions corresponding to the 30 mT demagnetization step (to simulate a bulk demagnetization). Site-level directions are determined using Fisher statistics (Fisher, 1953; under the assumption that directions should follow a Fisher distribution), then the mean between-site c_s is calculated for all sites with a $k_w \geq 50$ (any reverse polarity directions are converted to normal polarities). This process is repeated 1,000 times. The DC-4 simulation is the same except the directions for each randomly drawn sample are the characteristic remanent magnetizations from Mejia et al. (2004) and the site mean directions are calculated using Fisher statistics and the combined lines and planes method of McFadden et al. (1988).

Both DC-2 and DC-4 simulations are drawn from the same suite of available data, however DC-2 sites have a much larger variance in c_s than their DC-4 counterparts, with 95% bounds spanning about 4.5° for DC-2 compared to just over 1° for DC-4 sites (Figure 3a). Accepted DC-2 specimens (Figure 3b) show greater directional scatter and a larger number of specimens than those from the more restrictive DC-4 simulation (Figure 3c). The DC-4 method is inherently stricter in that it requires complete demagnetization, which allows researchers to exclude poorly behaved specimens, or to calculate characteristic mean directions using great circles (a common occurrence with AF demagnetization). The DC-2 method contains only a single demagnetization step which does not permit additional measurement level scrutiny and may hide rock magnetic and paleomagnetic peculiarities.

Although both DC-2 and DC-4 methods are statistically likely to represent the c_s of a given location, studies using the DC-2 method have a greater chance of incorrectly estimating directional dispersion by several degrees (Figure 3a). The median c_s value for DC-2 sites in Figure 3a is lower than the median c_s for DC-4 sites, but within the DC-4 95% confidence limits. Importantly, directional dispersion at the study level is variable and a lower c_s is not necessarily indicative of the "correct" value or methodology; what matters is that the resultant c_s is reliable. Our simulations indicate that the DC-4 demagnetization protocol substantially reduces the uncertainty in study-level c_s estimates, which is important because an error of several degrees can substantially affect the interpretation of subsequent geomagnetic field models. For this reason, we choose to exclude directional data derived from blanket demagnetization methods (DC-3 and lower) and focus the attention of PSV10 on high-quality sites obtained by complete specimen demagnetization (DC-4 or DC-5).

3. The PSV10 Compilation

3.1. General Selection Criteria

PSV10 is a collection of published directional studies on volcanic sites (i.e., lava flows, pyroclastic flows, and monogenetic centers) that meet three general criteria:

1. Studies must have applied modern demagnetization methods (DC-4 or DC-5, see Table 1).
2. Studies must not have explicitly targeted transitional field states.
3. The study area must be free of significant deformation (such as post-emplacement folding or faulting).

We used both electronic and print resources in our literature search, including the online MagIC database (https://earthref.org/MAGIC), online literature search engines, and previously published regional and global compilations of paleomagnetic data (such as Donadini et al., 2009; Johnson et al., 2008; Lawrence et al., 2006; McElhinny & McFadden, 1997). Every attempt was made to include only paleodirectional sites that accurately reflect the geomagnetic field; as a result, some studies were excluded from the compilation when demagnetization methods were not clearly stated (i.e., when we could not verify the use of principle component analysis) or if the study authors determined that the in situ integrity of their samples was compromised by tectonic effects and/or deformation. In instances in which a study reexamined or incorporated previously published material we included only the most recent publication to avoid duplicating directional sites (e.g., Antarctica, where Lawrence et al. (2009) built on previous work of Tauxe et al. (2004a) and Mankinen and Cox (1988), and the Boring Volcanic Field where Lhuillier et al. (2017) reanalyzed the work of Hagstrum et al. (2017)).

We found 81 studies (Table 2) that met all the above criteria and included them in our new PSV10 compilation. Figure 4 shows the location of each publication and reference numbers corresponding to Table 2. The global distribution of accepted studies is very similar to the original PSVRL compilation of McElhinny and McFadden (1997) (Figure 1a), but PSV10 displays a markedly improved spatial sampling when compared to only high-quality paleodirectional sites in PSVRL (Figure 1b) or to the more recent compilation of Johnson et al. (2008) (Figure 1c). PSV10 contains sites from each major continent with nearly continuous latitudinal coverage from Spitsbergen to Antarctica (references 1 and 81, respectively, Table 2 and Figure 4). Despite the improved global distribution of high-quality sites in PSV10, the northern hemisphere is preferentially sampled as is the longitudinal band through the Americas (reflecting targeted sampling in that region). Based on the geographic distribution of PSV10 studies, areas for future research should include central Asia, the western Pacific Rim, Africa, and both the Arctic and Antarctic, complemented by a global evaluation of ocean sediment records.

General statistics for PSV10 are shown in Figure 5. The earliest publication of an acceptable PSV10 study is Mitchell et al. (1989), after which the number of acceptable studies remains low until 1997. From the mid-1990s to present day there has been an average of about four high-quality paleodirectional publications per year except during 2008. The increase in accepted studies since about 1997 corresponds to a series of investigations modeling PSV and TAF behavior (e.g., Constable & Johnson, 1999; Constable & Parker, 1988; Johnson & Constable, 1996; Kono & Tanaka, 1995; McElhinny & McFadden, 1997; Quidelleur & Courtillot, 1996), and the community-wide recognition that accurate models of the geomagnetic field require a global distribution of high-quality directional data.

3.2. Additional Selection Criteria

Starting from the 81 PSV10 studies, we apply additional site selection criteria designed to improve overall data quality. Motivated by the results from Figures 2 and 3, we subselect those directional sites with at least four samples ($n \geq 4$) and a minimum within-site Fisher precision statistic, $k_w \geq 50$. In addition, all sites must have an average age of 10 Ma or younger.

3.3. Temporal Sampling

Average site ages and uncertainties vary by study, with the main differences being geochronology method and the level of detail about individual site ages provided in the original publication. Approximately 40% of the PSV10 sites have absolute ages derived from radiometric dating methods or historic records. We calculated average ages for sites without absolute dating estimates by taking the mean of stratigraphic and magnetic polarity constraints provided by the original authors. These estimated ages should be considered approximate because stratigraphic controls varied by study. Published sites listed as the same cooling unit, or interpreted to likely be the same unit during our literature review, were averaged together into a single directional site in PSV10. We account for any possible plate motion by rotating all sites to their original paleolatitude and longitude using the NNR-MORVEL model of Argus et al. (2011). Rotations are based on assigned average site ages described above. Paleosite changes are minimal with maximum paleolatitude and paleolongitude adjustments of about 1.4° and 4.8°, respectively. Site VGPs are recalculated for all site rotations and all statistical analyses of PSV10 sites in the following sections are performed using the plate-corrected locations and recalculated VGPs.

A remaining issue is how to deal appropriately with nonuniform temporal sampling and associated problems in trying to identify "typical stable polarity" field directions. There are three parts to this: (1) oversampling by paleomagnetists interested in geomagnetic excursions and transitional field states (which we address by excluding these studies); (2) oversampling by volcanic processes which can manifest as serial correlation in field directions (this question is addressed in section 4); (3) uneven temporal sampling of the long-term average field. This last question is not something that we can properly address at this time. Although a substantial number of records have absolute age estimates, ~60% do not, and many have substantial uncertainties (see supporting information Figures S1 and S2); it is therefore difficult to establish the extent of any temporal sampling bias in this data set. Good age constraints for future paleosecular variation studies are needed to properly evaluate this issue.

For studies accepted in PSV10, we do not exclude individual sites based on VGP colatitude, but we have explicitly excluded those studies or parts thereof that targeted excursional field states. For example,

Geochemistry, Geophysics, Geosystems

10.1002/2017GC007318

Table 2
Studies Included in the PSV10 Compilation

#	Lat	Lon	MLat	MLon	Age	*N*	N-SC	N-TB	Location	Reference	DOI
1	79.37	14.02	78.43	10.16	0.5–9.15	14	14	14	Spitsbergen	Cromwell et al. (2013a)	10.1002/ggge.20174
1	70.95	351.35	70.91	351.29	0–0.461	23	23	23	Jan Mayen	Cromwell et al. (2013a)	10.1002/ggge.20174
2	65.17	344.6	64.87	344.92	0.595–3.13	45	20	33	Iceland	Døssing et al. (2016)	10.1016/j.epsl.2016.09.022
3	65.07	344.48	64.78	344.8	0.78–1.82	17	13	15	Iceland	Udagawa et al. (1999)	10.1016/S0031-9201(99)00073-4
4	60	193.5	60.2	193.54	0.965	56	56	56	United States	Coe et al. (2000)[a]	10.1029/2007GC001696
5	53.24	190.1	53	190.66	0.075–2.06	84	6	13	United States	Stone and Layer (2006)[a]	10.1029/2005GC001007
6	51.47	237.65	51.51	237.72	0.002–0.76	51	26	38	Canada	Mejia et al. (2002)[a]	10.1029/2002GC000353
7	46.38	242.78	47.23	244.16	6.25–7.25	7	0	4	United States	Dominguez and Van der Voo (2014)	10.1093/gji/ggt487
8	46.01	238.23	46.21	238.49	0.008–3.25	20	20	20	United States	Mitchell et al. (1989)	10.1111/j.1365-246X.1989.tb00509.x
9	46.2	25.78	45.9	25.03	0.4–4.42	67	67	67	Romania	Panaiotu et al. (2012)	10.1111/j.1365-246X.2012.05394.x
10	45.96	25.35	45.87	25.12	0.535–1.14	20	19	20	Romania	Panaiotu et al. (2013)	10.1016/j.pepi.2013.06.007
11	45.52	237.7	45.68	237.9	0.059–3.249	69	69	69	United States	Lhuillier et al. (2017)	10.1093/gji/ggx288
12	45.52	2.81	45.52	2.81	0.008–0.012	6	6	6	France	Salis et al. (1989)	10.1029/JB094iB11p15771
13	44.98	4.15	43.74	2.2	7.95–9.7	8	8	8	France	Riisager et al. (2000)	10.1029/1999JB900337
14	42.99	246.4	43.14	246.64	0.052–5.75	22	22	22	United States	Tauxe et al. (2004b)[a]	10.1029/2003GC000661
15	41.68	43.94	41.57	43.52	0.31–2.29	41	41	41	Georgia	Goguitchaichvili et al. (2000)	10.1016/S1251-8050(00)01471-3
16	41.35	44.17	41.19	43.55	2–2.73	16	6	8	Georgia	Calvo-Rathert et al. (2011)	10.1016/j.pepi.2011.03.008
17	41.36	43.27	41.09	42.27	3.57–3.57	9	9	9	Georgia	Calvo-Rathert et al. (2013a)	10.1016/j.jseaes.2013.04.039
18	40.22	113.73	40.27	113.6	0.525	16	16	16	China	Yamamoto et al. (2007)	10.1186/BF03352736
19	38.59	331.22	38.59	−28.78	0.002–0.008	12	12	12	Azores	Di Chiara et al. (2014)	10.1130/B30933.1
20	38.38	14.97	38.37	14.95	0.1–0.135	39	1	4	Italy	Laj et al. (1997)	10.1016/S0031-9201(96)03221-9
21	38.16	140.47	38.22	140.35	0.1–1	9	9	9	Japan	Otake et al. (1993)	10.5636/jgg.45.595
22	37.81	334.62	37.75	334.56	0–0.878	33	33	33	Azores	Johnson et al. (1998)[a]	10.1016/S0012-821X(98)00117-4
23	37.82	358.47	36.94	357.26	2.61–8.2	10	10	10	Spain	Calvo-Rathert et al. (2009)	10.1186/BF03352885
24	35.87	137.49	35.95	137.33	0.393–0.73	20	20	20	Japan	Tanaka et al. (2007)	10.1111/j.1365-246X.2006.03306.x
25	35.91	137.49	35.91	137.47	0.021–0.084	35	25	26	Japan	Tanaka and Kobayashi (2003)[a]	10.1186/BF03351748
26	35.32	248.14	35.53	248.42	0.001–2.5	27	27	27	United States	Tauxe et al. (2003)[a]	10.1029/2002GC000343
27	28.78	342.11	28.65	341.99	0.39–1.79	22	22	22	Canary Islands	Tauxe et al. (2000)[a]	10.1029/2000GC000063
28	28.18	343.95	28.18	343.95	0–0.015	39	36	37	Canary Islands	Kissel et al. (2015)	10.1016/j.epsl.2014.12.031
29	28.33	343.14	27.45	342.29	5.7	26	16	18	Canary Islands	Leonhardt and Soffel (2006)	10.1007/s00531-006-0089-3
30	26.97	247.15	26.34	248.6	3	3	3	3	Mexico	Morales et al. (2003)	10.1016/j.crte.2003.07.002
31	21.67	254.8	22.43	255.64	8.9	45	1	2	Mexico	Goguitchaichvili et al. (2007)	10.1186/BF03352740
32	20.7	256.84	21.22	257.44	2.9–10	23	9	16	Mexico	Goguitchaichvili et al. (2011)	10.7288/V4/MAGIC/13117
33	21.31	202.21	21.22	202.4	0.033–0.677	14	14	14	Hawaii, USA	Herrero-Bervera and Valet (2002)	10.1016/S0031-9201(02)00092-4
34	20.98	255.65	21.19	255.89	0.307–4.01	7	7	7	Mexico	Calvo-Rathert et al. (2013b)	10.1007/s11200-012-0239-y
35	21.12	252.4	21.15	252.42	0.002–0.819	12	12	12	Mexico	Petronille et al. (2005)	10.1029/2004JB003321
36	20.84	256.06	20.88	256.11	0.115–1.13	16	16	16	Mexico	Ceja et al. (2006)	10.1186/BF03352631
37	20.37	257.68	20.72	258.1	0.5–10	41	41	41	Mexico	Ruiz-Martinez et al. (2010)	10.1111/j.1365-246X.2009.04447.x
38	21.56	201.75	20.67	203.57	3.1–3.19	98	0	4	Hawaii, USA	Laj et al. (1999)	10.1016/S0012-821X(99)00119-3
39	21.32	202.2	20.65	203.55	1.8–2.6	9	9	9	Hawaii, USA	Herrero-Bervera and Valet (2003)	10.1016/S0012-821X(03)00168-7
40	20.65	203.66	20.63	203.69	0.001–0.703	12	12	12	Hawaii, USA	Herrero-Bervera and Valet (2007)	10.1016/j.pepi.2007.02.008
41	20.81	203.08	20.54	203.63	0.86–1.12	7	7	7	Hawaii, USA	Herrero-Bervera et al. (2000)	10.1016/S0377-0273(00)00197-9
42	20.16	262.81	20.39	263.17	1.53–7.33	14	14	14	Mexico	Goguitchaichvili et al. (2002)	10.1016/S0031-9201(02)00096-1
43	20.14	258.71	20.28	258.88	0.56–2.78	11	8	10	Mexico	Peña et al. (2011)	10.1007/s11200-011-0017-2
44	20.14	204.18	20.07	204.32	0.061–0.4	10	10	10	Hawaii, USA	Brassart et al. (1997)	10.1016/S0012-821X(97)00024-1
45	19.83	260.36	19.94	260.51	1.28–4.14	12	12	12	Mexico	Mejia et al. (2005)[a]	10.1029/2004GC000871
46	19.87	101.58	19.87	−101.55	0–3.53	32	32	32	Mexico	Michalk et al. (2013)	10.1002/jgrb.50214
47	19.68	258.19	19.72	258.24	0–2.1	22	22	22	Mexico	Conte-Fasano et al. (2006)	10.1186/BF03352632

Geochemistry, Geophysics, Geosystems

10.1002/2017GC007318

Table 2. (continued)

#	Lat	Lon	MLat	MLon	Age	*N*	N-SC	N-TB	Location	Reference	DOI
48	19.53	204.76	19.53	204.76	0.003–0.028	8	8	8	Hawaii, USA	Valet et al. (1998)	10.1016/S0012-821X(98)00133-2
49	19.35	259.67	19.35	259.68	0–0.029	11	11	11	Mexico	Gonzalez et al. (1997)	10.1111/j.1365-246X.1997.tb00999.x
50	19.33	260.83	19.33	260.83	0.002	10	1	2	Mexico	Alva-Valdivia (2005)	10.1186/BF03351862
51	19.11	258.44	19.19	258.54	0.003–4.18	30	30	30	Mexico	Peña et al. (2014)	10.1016/j.pepi.2014.01.005
52	19.14	260.77	19.14	260.77	0.002–0.039	7	7	7	Mexico	Morales et al. (2001)	10.1186/BF03351686
53	18.78	249.07	18.72	249.21	0.283–0.283	7	7	7	Mexico	Sbarbori et al. (2009)	10.1186/BF03352899
54	18.42	264.83	18.51	264.99	0.8–3.1	9	9	9	Mexico	Alva-Valdivia et al. (2001)	10.1186/BF03351684
55	17.08	334.72	17.02	334.64	0.451–0.477	27	1	4	Cape Verde	Brown et al. (2009)	10.1016/j.epsl.2009.07.039
56	16.03	298.32	15.97	298.27	0.047–1.02	23	23	23	West French Indies	Carlut et al. (2000)	10.1029/1999JB900238
57	14.73	298.66	14.6	298.54	0.01–2.27	14	14	14	Martinique	Tanty et al. (2015)	10.1093/gji/ggu423
58	10.14	275.62	10.13	275.58	0.005–2.11	30	23	23	Costa Rica	Cromwell et al. (2013b)[a]	10.1002/ggge.20199
59	4.94	284.62	4.9	284.65	0–2.65	46	46	46	Columbia	Sánchez-Duque et al. (2016)	10.1002/2015GC006149
60	2.8	36.73	2.12	35.78	3.53–4.84	33	33	33	Kenya	Opdyke et al. (2010)	10.1029/2009GC002863
61	0.29	6.62	−0.05	6.23	0.5–5.5	38	38	38	Sao Tome	Opdyke et al. (2015)	10.1002/2015GC005901
62	−0.41	281.73	−0.48	281.78	0.018–2.71	50	50	50	Ecuador	Opdyke et al. (2006)	10.1029/2005GC001221
60	0.06	37.59	−0.53	36.77	0.3–5.36	60	60	60	Kenya	Opdyke et al. (2010)	10.1029/2009GC002863
63	−0.95	269.94	−1.08	269.18	1.5	53	53	53	Galapagos Islands	Kent et al. (2010)	10.1016/j.pepi.2010.08.010
64	−3.86	327.57	−4.35	327.77	2.55–10	38	27	29	Fernando de Noronha	Leonhardt et al. (2003)	10.1016/j.pepi.2003.09.008
65	−7.55	112.23	−7.45	111.98	0–6.7	46	43	44	Indonesia	Elmaleh et al. (2004)	10.1111/j.1365-246X.2004.02197.x
66	−16.93	208.99	−17.68	210.54	0.905–4.21	123	54	70	Society Islands	Yamamoto et al. (2002)	10.1186/BF03351733
67	−21.09	55.47	−21.1	55.45	0.073-0.131	38	0	2	Reunion Island	Rais et al. (1996)	10.1016/0012-821X(96)00024-6
68	−21.22	55.66	−21.23	55.66	0.009–0.09	23	1	4	Reunion Island	Chauvin et al. (1991)	10.1029/90JB02223
69	−27.1	250.67	−27.08	250.41	0.06–0.4	27	27	27	Easter Island	Miki et al. (1998)	10.1016/S0031-9201(97)00106-4
70	−35.27	289.48	−35.29	289.48	0.275	8	8	8	Argentina	Canon-Tapia et al. (1994)	10.5636/jgg.46.143
71	−36.09	290.88	−36.15	290.87	0.007–1.72	30	30	30	Argentina	Quidelleur et al. (2009)	10.1016/j.pepi.2008.09.012
72	−38.16	176.5	−38.16	176.5	0–0.021	13	13	13	New Zealand	Tanaka et al. (2009)	10.1186/BF03352901
73	−37.66	144.28	−38.67	143.81	2.63–2.63	37	37	37	Australia	Opdyke and Musgrave (2004)[a]	10.1029/2003GC000632
74	−38.91	288.26	−38.91	288.26	0–0.005	18	11	13	Chile	Roperch et al. (2015)	10.1016/j.pepi.2015.03.005
75	−39.23	175.6	−39.29	175.59	−0.024 to 0.292	24	4	7	New Zealand	Tanaka et al. (1997)[a]	10.5636/jgg.49.587
76	−46.41	51.79	−46.46	51.47	0.64–3	37	3	7	Possession Island	Camps et al. (2001)	10.1029/2000JB900370
77	−46.99	288.88	−47.1	288.81	0.034–7.86	32	29	32	Patagonia	Brown et al. (2004)[a]	10.1029/2003GC000526
78	−51.21	289.37	−51.39	289.24	0.165–8.67	37	24	31	Patagonia	Mejia et al. (2004)	10.1029/2003GC000633
79	−62.95	299.33	−62.95	299.31	0.05	17	17	17	Deception Island	Oliva-Urcia et al. (2016)	10.1007/s00531-015-1254-3
80	−62.97	299.34	−62.97	299.32	0.075–0.075	18	18	18	Deception Island	Baraldo et al. (2003)	10.1046/j.1365-246X.2003.01881.x
81	−77.94	165.11	−77.71	164.36	0.026–9.02	128	128	128	McMurdo, Antarctica	Lawrence et al. (2009)	10.1029/2008GC002072

Note. # is the study number, corresponds to study locations in Figure 4. Lat and Lon are average latitude (north) and longitude (east) for each study, and MLat and MLon are average of plate-corrected latitude (north) and longitude (east). Age is the range of average site ages (Ma) of all study sites. *N* is the number of sites at each study location in PSV10; N-SC, and N-TB are the number of sites for the PSV10-SC and PSV10-TB data sets. Location is the general study location. Reference is the short study name. DOI is the digital object identifier unique to each study.

[a]See also Johnson et al. (2008).

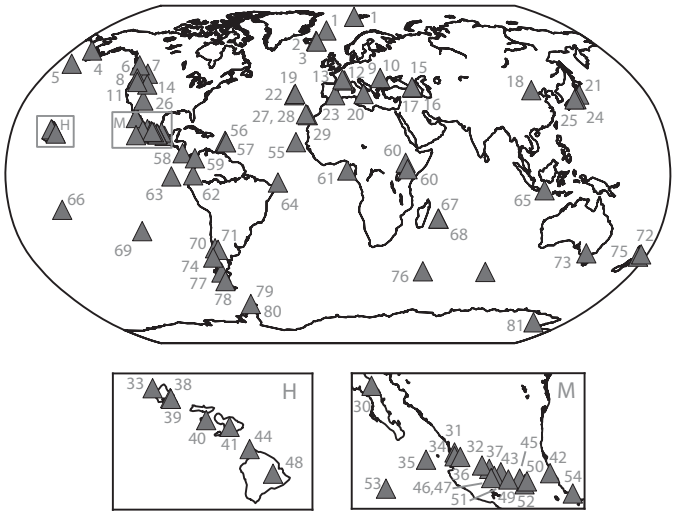

Figure 4. PSV10 study locations. Numbers correspond to the study numbers listed in Table 2. Lower insets are enlargements of Hawaii (H) and Mexico (M).

Panaiotu et al. (2013) preferentially sampled a series of lavas emplaced during the Cobb Mountain normal polarity subchron as part of their paleosecular variation study in the Persani Mountains, and subsequently reported some transitional directions. We chose to keep the Panaiotu et al. (2013) study in PSV10, but we excluded sites that were from the targeted subchron sampling effort. Although exclusion of transitional studies is an imperfect solutions we can assess its impact by making a crude estimate of the percentage of time the field might spend in transition, and comparing this with the percentage of such sites in PSV10. Using marine sediment records Clement (2004) finds average transition times of 7,000 years for the past four reversals. Assuming this to be also representative of reversals over the past 10 Ma (Cande & Kent, 1995), we might expect the field to be in an excursional state about 3% of the time. Using our selection criteria, ~4% of all sites in PSV10 would be considered transitional when a VGP colatitude cutoff of 45° is applied. The two estimates are similar which could indicate that PSV10 effectively captures long-term trends in the geomagnetic field, bearing in mind the nonuniform temporal sampling evident in Figure 5, and that the sediment-based estimate of Clement (2004) excludes multiple excursions that will appear in the PSV10 data set.

A total of 2,401 directional sites meet our requirements and Figure 5b shows the age distribution for the entire collection. PSV10 is weighted to the last five million years (N_{5Ma} = 2,235) with most sites emplaced during the Brunhes (N_B = 982) and Matuyama Chrons (N_M = 764).

4. Serial Correlation of Lavas

Analyses of long-term geomagnetic field behavior, such as paleosecular variation and the time-averaged field, assume that individual paleomagnetic data points can be considered uniformly sampled over time. If a certain time period is oversampled, those data are likely to be serially correlated and may bias any PSV or TAF calculations. Oversampling of the geomagnetic field can be minimized by sampling volcanic units with distinct radiometric or stratigraphic age differences, and by not sampling entire stacks of lava flows.

Several studies included in PSV10 addressed the issue of serial correlation and employed various methodologies in an attempt to remove any potential sampling bias. To ensure consistency across all PSV10 studies, we considered sites from consecutive or stacked lava flows to be serially correlated, regardless of any analysis (or lack thereof) performed by the original authors. We searched all 81 publications for sites that were sampled from a single lava flow sequence and generated two modified data sets: PSV10-SC and PSV10-TB. In PSV10-SC (SC = corrected for serial correlation) directions of all sites from the same stack of consecutive lavas were averaged to represent a single site mean, reflecting the assumed short time period in which those lavas were likely emplaced. Averaging successive lava flows may remove the oversampling bias if the lava flows erupted in a short time span and if secular variation of the geomagnetic field was limited. It is also possible that this averaging process could suppress secular variation if geomagnetic field variations occurred rapidly, or if the sequences represent substantial periods of time. To address this possibility, we adopted an alternative geologic field sampling approach to correct for serial correlation in PSV10-TB (TB = top and bottom). Rather than averaging all sites in a lava stack, we selected only the top and bottom flows in each lava sequence and removed all others. This assumes that the top and bottom flows of any sequence are the most distant in time and are more likely to represent different geomagnetic field states.

Twenty-eight studies in PSV10 are partially, or completely composed of serially correlated lava flows and contain a total of 94 lava flow sequences (sequential normal and reverse polarity lavas from the same stack were averaged separately). Mean directions of 20 of these sequences did not pass our k_w criterion and were therefore excluded from further analysis. These low k_w sequences may contain uncorrelated directions emplaced over an extended time duration, but we prefer to maintain a simple, conservative approach to this issue in the PSV10-SC data set; less stringent criteria is applied in PSV10-TB. Summary statistics for PSV10-SC and

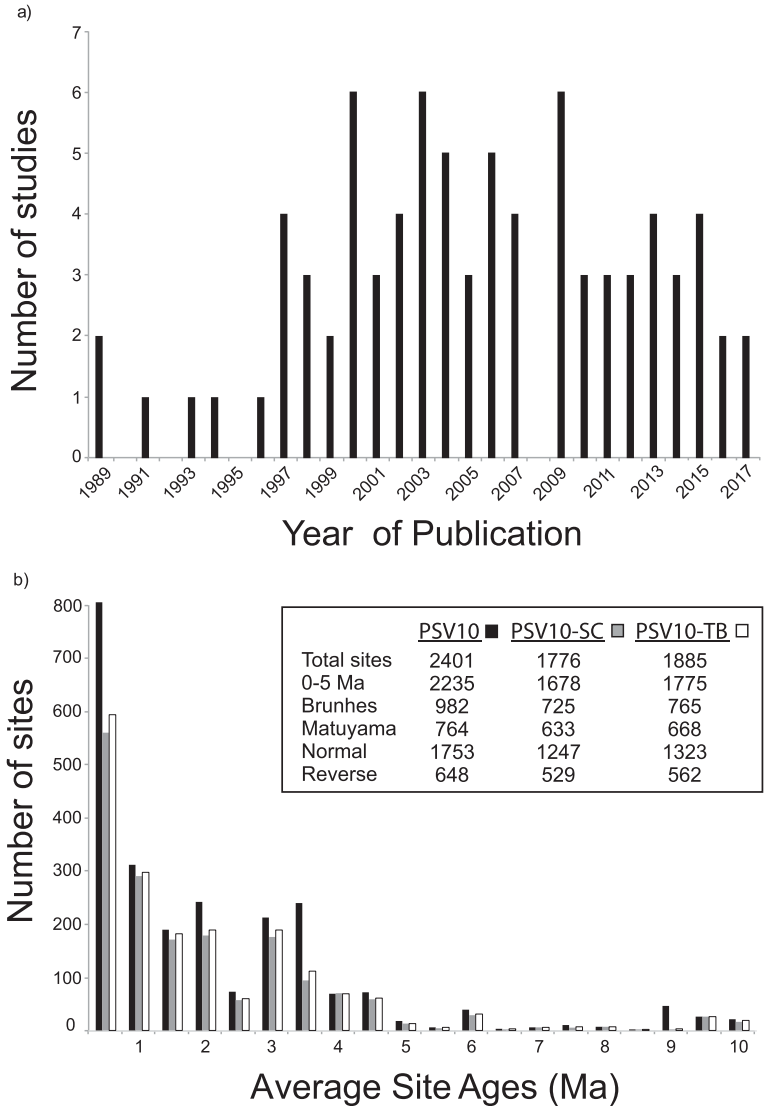

Figure 5. General statistics of the PSV10 compilation. (a) Distribution of the number of PSV10 studies and their year of publication. (b) Age distribution of all PSV10 (black), PSV10-SC (gray), and PSV10-TB (white) sites in 0.5 Myr intervals.

PSV10-TB are shown in Figure 5b. PSV10-SC and PSV10-TB contain a substantially reduced number of sites compared to the original PSV10 data set, with a total of 1,776 sites in PSV10-SC, and 1,885 in PSV10-TB.

5. Inclination Anomaly and VGP Dispersion From PSV10 Data

In this section, we analyze various subsets of data drawn from PSV10 to identify signals arising from zonal TAF field structure and PSV, and we assess whether zonal models provide an adequate fit to the observations. Both TAF and PSV statistics, in the form of average inclination anomaly, $\overline{\Delta I}$, and VGP dispersions, S_F, grouped by 10° latitude bins, are compared with model TK03, and VGP dispersions with Model G.

S_F for Model G (McElhinney & McFadden, 1997) is calculated (equation (1)) at the same mean latitude as the data for each bin. For TK03, we generated 10,000 paleomagnetic directions at each of the same mean latitudes using model parameters set in tk03.py (part of the PmagPy software package (Tauxe et al., 2016), available using instructions at https://earthref.org/PmagPy/cookbook/). We then generated VGP latitude and longitude pairs for each direction and calculated S_F (both with and without the iterative VGP cutoff;

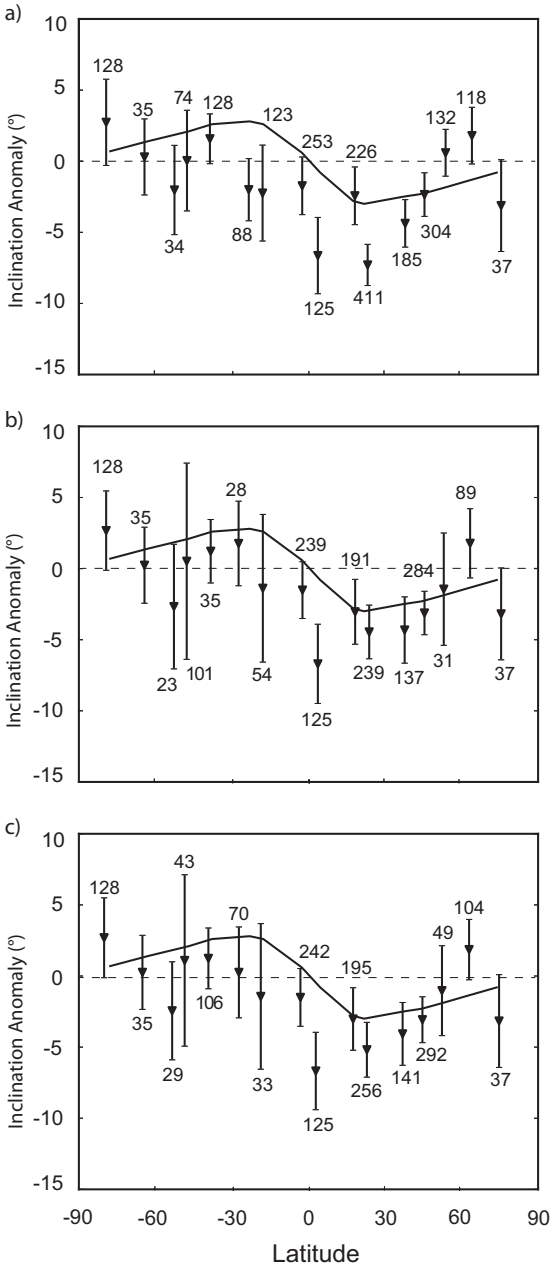

Figure 6. Average inclination anomaly in degrees for (a) PSV10, (b) PSV10-SC, and (c) PSV10-TB. Inclination anomaly values for all figures calculated for 10° latitude bins and plotted with bootstrapped 95% confidence bounds and the number of sites in each bin. Predicted inclination anomalies for a GAD field (short dashed line) and TK03 (solid black line) are also plotted.

Vandamme, 1994) from those 10,000 VGP pairs. In computing S_F for the actual data sets described below, we correct for within-site uncertainty (McElhinny & McFadden, 1997):

$$S_F = \sqrt{(N-1)^{-1}\sum_{i=1}^{N}\left((\Theta_i)^2 - \frac{{S_{w_i}}^2}{n_i}\right)}, \quad (2)$$

where N is the number of sites, Θ_i is the angle between the ith VGP and the spin axis, S_{w_i} is within-site scatter (defined as $81°/\sqrt{k_w}$, where k_w is the Fisherian precision statistic), and n_i is the number of samples at the ith site.

For the TAF model, Fisher mean inclinations were calculated for each latitude grouping of directions and the inclination predicted by GAD subtracted to yield the mean inclination anomaly, $\overline{\Delta I}$. $\overline{\Delta I}$ values are compared with GAD ($\overline{\Delta I} = 0$) and with the prediction of TK03. The underlying TAF in TK03 is GAD, however, the variability in the field imparted by the statistical description of PSV, together with the calculation of $\overline{\Delta I}$ from directions only instead of the full paleomagnetic vector results in a nonzero $\overline{\Delta I}$ as discussed previously in the literature (Creer, 1983; Johnson et al., 2008).

For each collection of S_F and ΔI, we calculated the square root of the weighted χ^2 misfit value to both TK03 and Model G. The weights used are one standard deviation about the average value, and we call these statistics χ_{SF} and χ_{IA}. These values of χ are compared with χ_{95}, the 95% confidence limit on the expected value of χ^2 to determine whether the overall fit to a specific model is adequate.

We examine several subsets of the data and corresponding terminology so that we can assess the impact of sampling of transitional field behavior and of serial correlation on our results. The various subsets are listed below, and the main results for discussion are shown in Figures 6–8 and Table 3.

1. PSV10: Combined polarity, all data in PSV10.
2. PSV10$_N$: All normal polarity.
3. PSV10$_R$: All reverse polarity.
4. PSV10$_{vcut}$: Combined polarity, VGP cutoff following criteria of Vandamme (1994).
5. PSV10-SC: Combined polarity, corrected for serial correlation, i.e., PSV10-SC.
6. PSV10-SC$_N$: Normal polarity, corrected for serial correlation.
7. PSV10-SC$_{vcut}$: Combined polarity, corrected for serial correlation, VGP cutoff following criteria of Vandamme (1994).
8. PSV10-TB: Combined polarity, top and bottom, i.e., PSV10-TB.
9. PSV10-TB$_N$: Normal polarity, corrected for serial correlation.
10. PSV10-TB$_{vcut}$: Combined polarity, corrected for serial correlation, VGP cutoff following criteria of Vandamme (1994).

5.1. Combined Polarity Results: Inclination Anomaly

The time-averaged inclination anomalies, $\overline{\Delta I}$, recorded by the PSV10 data set are shown in Figure 6a. PSV10 has latitudinal data coverage from the Antarctic to the Arctic, although the mid-Southern Hemisphere and Arctic regions contain substantially fewer sites than other regions (see also Figure 4). While many of these inclination anomalies are consistent at the 95% confidence limit with a GAD field ($\overline{\Delta I} = 0°$), there are significant deviations from GAD in latitude bands spanning 0°N–50°N. With the exception of the adjacent 30°N–40°N and 40°N–50°N latitude bands, there is also substantial variability in $\overline{\Delta I}$ between neighboring bins indicating that TAF estimates for the northern hemisphere are not easily modeled by a zonal field. The 70°S–80°S bin (Antarctica) has a large

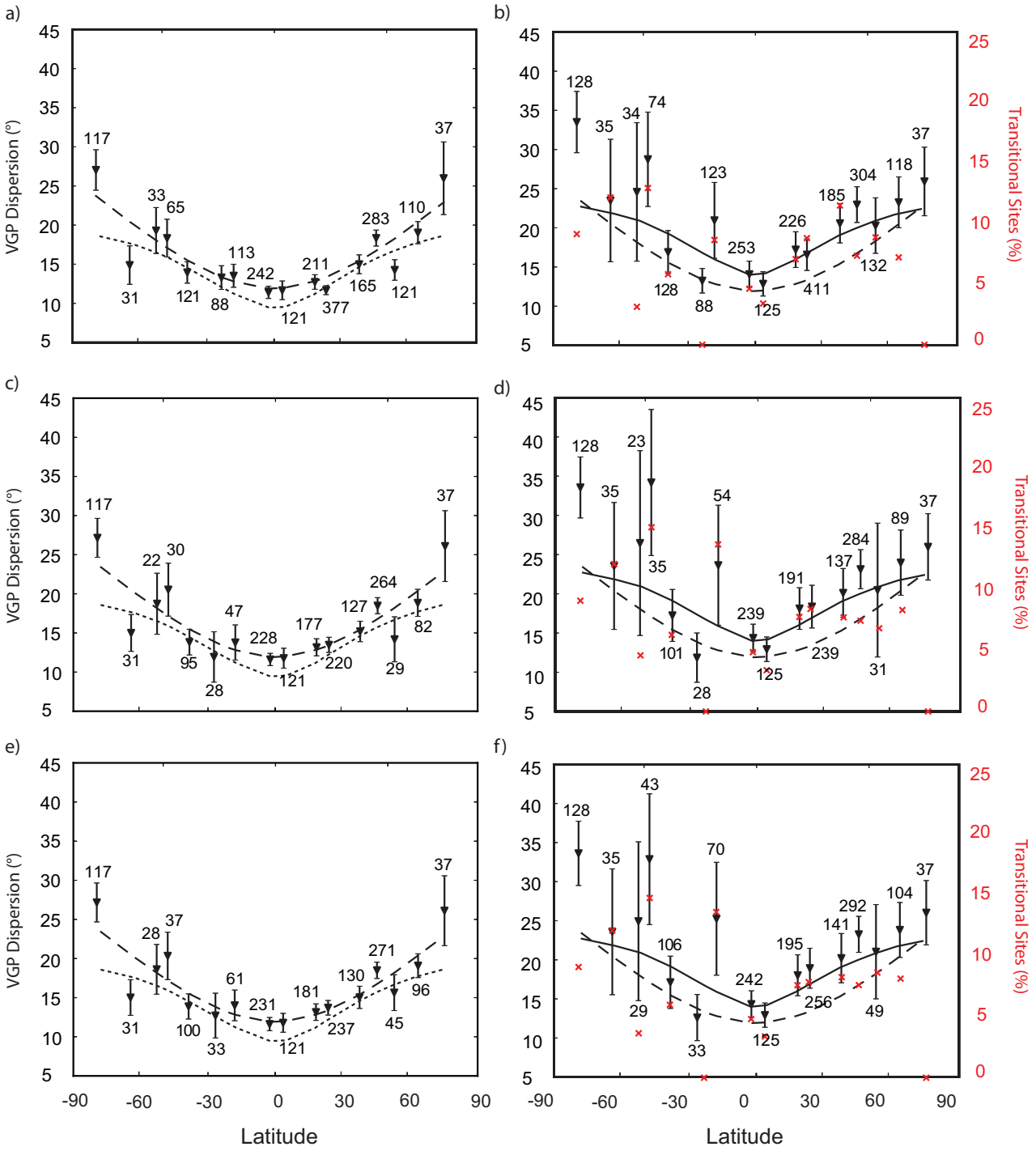

Figure 7. Average VGP dispersion (S_F) for combined polarity data sets (a, b) PSV10, (c, d) PSV10-SC, and (e, f) PSV10-TB. VGP dispersion using the iterative Vandamme VGP cutoff criterion is shown in the left column (Figures 7a, 7c, and 7e), while VGP dispersion with no cutoff criterion is shown in the right column (Figures 7b, 7d, and 7f). Dispersion values are calculated for 10° latitude bins and shown with bootstrapped 95% confidence bounds and the number of sites in each bin. Predicted VGP dispersion values for Model G (long dashed line), TK03 (solid line), and TK03 with Vandamme cutoff (short dashed line in Figures 7a, 7c, and 7e) are also shown. Red marks in Figures 7b, 7d, and 7f show the percentage of transitional sites in each latitude bin relative to Vandamme VGP cutoff.

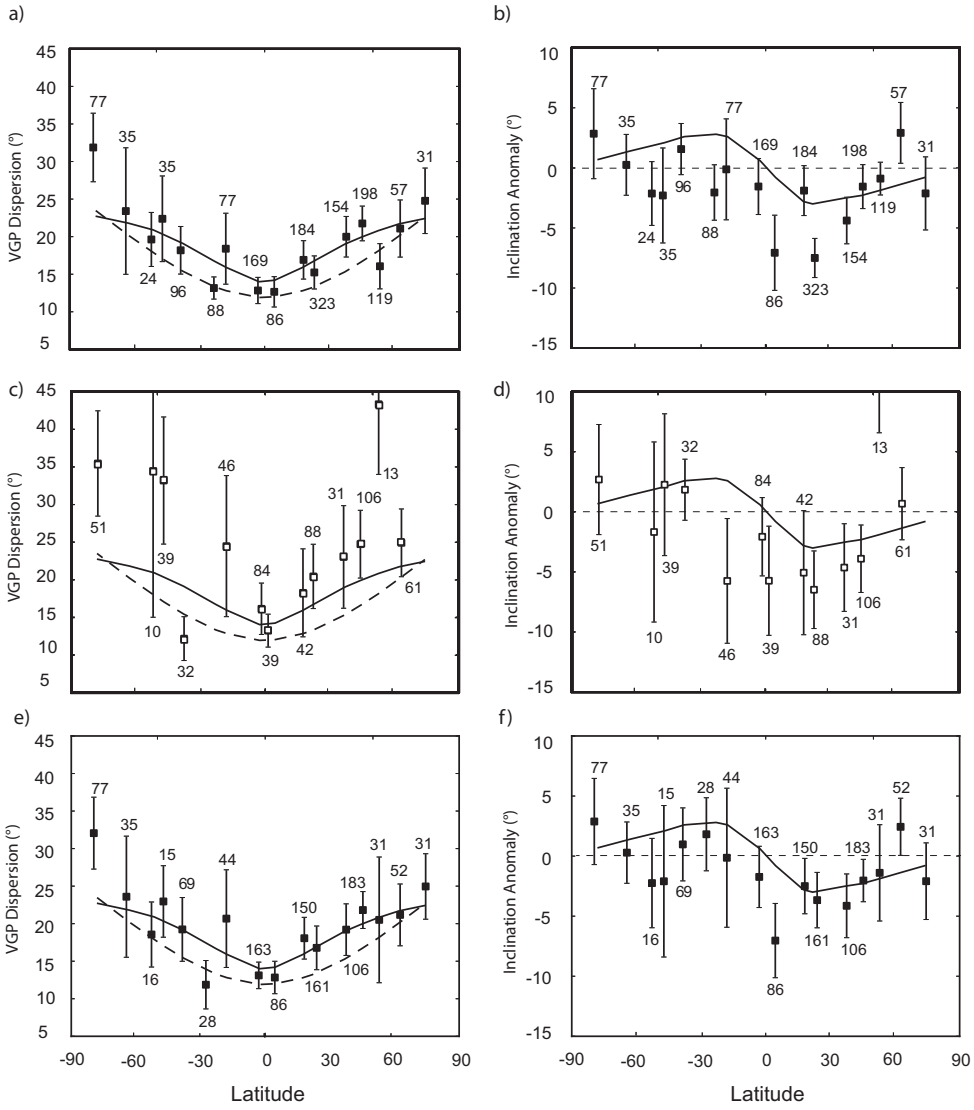

Figure 8. Average VGP dispersion (S_F) and inclination anomaly (ΔI), in degrees, for (a, b) normal and (c, d) reverse subsets of PSV10, and (e, f) normal polarity subset of PSV10-SC. VGP dispersion and inclination anomaly values for all figures calculated for 10° latitude bins, and plotted with bootstrapped 95% confidence bounds and the number of sites in each bin. Predicted VGP dispersion values for Model G (long dashed line) and TK03 (solid black line) are shown, as well as predicted inclination anomalies for a GAD field (short dashed line) and TK03 (solid black line).

positive $\overline{\Delta I}$ that is more consistent with, e.g., a nonzero axial-octupole ($\bar{g}_3^0$) term, such as that predicted by the statistical variability in TK03 (Johnson et al., 2008) but larger in amplitude, or alternatively a non-GAD regional signature in the TAF. The misfits, χ_{IA}, of $\overline{\Delta I}$ to TK03 and GAD are 3.0 and 3.5, respectively.

The inconsistencies between consecutive latitude bands and the inability of TK03 to fit the inclination anomalies in the data set are suggestive of regional structure in the long-term geomagnetic field. For example, Hawaii and Mexico have a large number of sites (158 and 305, respectively) and the same average latitude (∼20.5°N), but are almost 40° apart in longitude (Figure 4). Mexico has a $\overline{\Delta I}$ of $-3.6 \pm 1.5°$, consistent with TK03, but Hawaii has a $\overline{\Delta I}$ of $-9.0 \pm 2.0°$ that, if fit with a zonal field, would likely require a substantial $\bar{g}_2^0$ contribution (e.g., 5–10%). The differences in TAF behavior in Hawaii, Mexico, and other highly sampled regions have been well documented (Johnson et al., 2008; Lawrence et al., 2006) and highlight the difficulty of predicting global TAF (and PSV) behavior with a zonal statistical model.

Table 3
Square Root of the Reduced χ^2 Misfits of Model G and TK03 to VGP Dispersion Estimates (χ_{SF}) and Inclination Anomalies (χ_{IA}) for the PSV10, PSV10-SC, and PSV10-TB Data Sets

Data set	χ_{SF} (Model G)	χ_{SF} (TK03)	χ_{IA} (TK03)	χ_{95}
PSV10	3.2	2.4	3.1	1.3
PSV10 $_N$	2.4	2.1	2.8	1.3
PSV10$_R$	3.1	2.8	2.2	1.3/1.4
PSV10$_{vcut}$	3.0	3.6		1.3
PSV10-SC	3.0	2.3	1.9	1.3
PSV10-SC$_N$	2.3	1.7	1.8	1.3
PSV10-SC$_{vcut}$	2.1	3.6		1.3
PSV10-TB	3.1	2.3	2.1	1.3
PSV10-TB$_N$	2.4	1.7	1.9	1.3
PSV10-TB$_{vcut}$	2.1	3.6		1.3

Note. Subscripts *N*, *R* denote normal and reverse polarity subsets and *vcut* denotes the subsets of each data set retained after removal of transitional sites (Vandamme, 1994). χ_{95} values are the 95% confidence limit on the expected value of χ (the expected 95% confidence limit is the same for Model G and TK03, except for the reverse PSV10 data set where the limit is 1.3 for Model G and 1.4 for TK03). Only χ_{SF} misfit values were calculated for *vcut* datasets.

The influence of serial correlation is demonstrated in Figures 6b and 6c. The corrected PSV10-SC and PSV10-TB data sets generally show minor differences in the values of $\overline{\Delta I}$ compared with the full PSV10 data set, reflecting an average reduction of 3–50 sites per latitude band in the two corrected data sets. Three latitude bins have a substantial number of sequential lava flows, indicated by the reduced number of sites in the SC and TB data sets: 50°N–60°N, 20°N–30°N, and 10°S–20°S. The greatest difference in $\overline{\Delta I}$ between PSV10 and PSV10-SC or PSV10-TB occurs in the 20°N–30°N latitude bin. This observation indicates the importance of regional correction for serial correlation for studies with a large number of sequentially sampled lava flows. Although the overall global fits of PSV10-SC ($\chi_{IA} = 1.9$) and PSV10-TB ($\chi_{IA} = 2.1$) to TK03 improve compared to PSV10, $\chi_{IA} = 3.1$) they still do not meet the χ_{95} threshold for an adequate fit. The lack of a clear zonal signal in the TAF for $\overline{\Delta I}$ suggests that TK03 needs modification from the vector average TAF corresponding to GAD. This also has some visible consequences for the signal in S_F as we see below.

5.2. Combined Polarity Results: VGP Dispersion

VGP dispersion results are presented as a function of latitude in Figure 7 for data sets PSV10, PSV10-SC, and PSV10-TB, and their respective subsets calculated using the Vandamme (1994) VGP cutoff criterion, PSV10$_{vcut}$, PSV10-SC$_{vcut}$, and PSV10-TB$_{vcut}$. The corresponding χ_{SF} values for the comparisons of the data sets with TK03 and Model G are given in Table 3. Departures between existing PSV model predictions and our observations might be expected because the directional sites in PSVRL, from which TK03 and Model G were derived, differ greatly from PSV10 in quality and distribution in space and time. Furthermore, the paucity of Southern Hemisphere data in PSVRL encouraged the authors of TK03 and Model G to enforce north/south hemispheric symmetry by fitting S_F versus absolute latitude.

PSV10$_{vcut}$ provides the best visual fit to TK03 and Model G predictions (Figure 7a). This is to be expected because the Vandamme VGP cutoff criterion was used in constructing both PSV models from the earlier PSVRL data set. However, the observed PSV10$_{vcut}$ dispersion is generally higher than that predicted by TK03, and Model G performs better overall. S_F and its 95% confidence limits increase when transitional sites are included (Figure 7b), and this is particularly noticeable when the percentage of transitional sites is more than a few percent and/or when the number of sites is small. S_F shows an overall increase with latitude, consistent with previous studies, although the amplitude of S_F here may be more pronounced. TK03 fits the observed PSV10 dispersion reasonably well at the equator and at most northern hemisphere latitude bands (Figure 7b), but underestimates S_F in most Southern Hemisphere latitude bands, especially in Antarctica. Model G shows a general latitudinal increase, consistent with our data set, but on average is too low at all latitudes, reflecting the fact that it does not predict field variability associated with transitional sites. Neither TK03 nor Model G fits the observed dispersion (Table 3). After correction for serial correlation, larger uncertainties estimates, but only minimal changes in mean S_F values are seen (Figures 7c and 7d). The χ_{SF} values (Table 3) indicate that PSV10-SC and PSV10-TB are also not fit by existing PSV models.

A perhaps surprising result from PSV10 is the substantially larger increase in S_F with latitude in the Southern Hemisphere compared with in the north, predicted by Cromwell et al. (2013a). As this behavior is also observed in PSV10-SC and PSV10-TB, we infer that VGP dispersion has not been artificially suppressed in the northern hemisphere in PSV10 due to oversampling of short periods with low PSV through the inclusion of sections with possible serial correlation. However, north/south differences in VGP dispersion in PSV10 (Figure 7b) are, for the most part, removed when the Vandamme cutoff filter is applied (Figure 7a). The percentage of transitional sites is quite variable from one latitude band to another (Figure 7). If these percentages reflect real variations in field behavior from one location to another (as the percent of transitional directions in PSV10 might indicate, section 3.3), simple modifications to the parameters of TK03 might describe the observed asymmetry in S_F seen in PSV10, PSV10-SC, and PSV10-TB. Three parameters in TK03 describe the statistical distributions of the g_l^m and h_l^m, and hence the statistical distributions of the resulting paleomagnetic vectors. They are the average axial-dipole term $\bar{g}_1^0$, plus α and β which describe the variance

in the Gauss coefficients: α^2 is proportional to the variance (σ_l^2) in the symmetric family of Gauss coefficients of degree l (Constable & Parker, 1988). β is defined as the ratio between the variance in the equatorially antisymmetric and symmetric families of Gauss coefficients (Tauxe & Kent, 2004) and determines the scale of the latitudinal dependence of S_F. Modification to these parameters has no effect on the north/south asymmetry in S_F; that can be influenced by changes to the time-averaged values for the individual Gauss coefficients. The actual strength of the average axial-dipole term in TK03 has no impact on VGP scatter; it is the ratio of other TAF terms to $\bar{g}_1^0$ that matters. Introducing a nonzero $\bar{g}_2^0$ contribution ranging from 0 to 20% of g_1^0 produces an asymmetry in S_F, but has the wrong latitudinal dependence in $\overline{\Delta I}$ to explain the TAF structure discussed in the previous section. Alternatively, a nonzero value of $\bar{g}_3^0$ might help explain some of the $\overline{\Delta I}$ signal but will not resolve the asymmetry in S_F. We explored a range of empirical modifications to TK03 parameters but were unable to find a suitable combination that reduced the misfit level for S_F or $\overline{\Delta I}$ to lie within the range expected by χ_{95}. We infer that a non-zonal TAF is needed at least to explain $\overline{\Delta I}$ and possibly for S_F too.

5.3. Differences Between Normal and Reverse Polarity Data

Normal and reverse polarity intervals have repeatedly been shown to record significantly different average geomagnetic field behaviors (see e.g., Merrill & McElhinny, 1977 for TAF structure and Ziegler et al., 2011 for paleointensity). Accordingly, they may be best treated separately (Johnson & Constable, 1996). Most regions represented in the PSV10 collection contain both normal and reverse polarity data although there are nearly three times as many normally magnetized sites (Figure 5b), with normal (reverse) polarity data dominated by Brunhes (Matuyama) aged sites, respectively.

We evaluate S_F and ΔI for three polarity based subsets of the data: PSV10$_N$ (Figures 8a and 8b), PSV10$_R$, (Figures 8c and 8d), and PSV10-SC$_N$ (Figures 8e and 8f). We do not discuss the normal polarity subset of PSV10-TB as it has almost identical behavior to PSV10-SC$_N$ (Table 3). We also do not discuss the reverse polarity subset of PSV10-SC because of the more limited number of data. We compare these data sets with TK03 and Model G and provide the χ_{SF} and χ_{IA} misfits to these models in Table 3.

S_F is lower overall for PSV10$_N$ than for PSV10 and has an improved fit to TK03 ($\chi_{SF} = 2.1$), however, the misfit still exceeds the 95% confidence limit. VGP dispersion is more variable and larger overall for PSV10$_R$ and the misfit to TK03 ($\chi_{SF} = 2.8$) is correspondingly larger. These observations are consistent with previous studies (e.g., Johnson & Constable, 1996; Johnson et al., 2008) and may reflect the lower average field strength during the Matuyama than in the Brunhes Chron (e.g., Ziegler et al., 2011). The high-quality nature of PSV10 sites ensures that reverse paleomagnetic directions are not contaminated by viscous overprints and the increased variance in S_F during reverse polarities, dominated in this data set by Matuyama versus Brunhes, is likely a real feature of the long-term geomagnetic field.

Inclination anomalies for PSV10$_N$ and PSV10$_R$ (Figures 8b and 8d) do not show a well-defined latitudinal structure and we observe no systematic difference between the two polarities for data in the same latitude bins. In several latitude bins $\bar{\Delta}I$ is consistent with no anomaly at the 95% confidence level, but elsewhere (most notably some midnorthern latitude bins containing many data) lies closer to TK03. It is clear from Figures 8b and 8d that there is no simple statistical zonal model that can predict $\bar{\Delta}I$ behavior for either polarity subset.

Finally, we note that S_F and $\bar{\Delta}I$ for PSV10-SC$_N$ (Figures 8e and 8f) are similar to those for PSV10$_N$ (Figures 8a and 8b) but have a substantially improved (albeit still unsatisfactory) fit to TK03, especially in the northern hemisphere. The effect of serially correlated lava flows is more pronounced between the PSV10$_N$ and PSV10-SC$_N$ subsets of PSV10, than between the PSV10 and PSV10-SC data sets (Figures 6 and 7 and Table 3). This is in part due to the fact that most of the sequential lava flows in PSV10 are normal polarity but is also indicative of the substantially different, and more variable, geomagnetic field behavior observed in the reverse polarity data (Figures 8b and 8c).

6. Non-zonal Time-Averaged Field Structure

Motivated by the significant improvement in the spatial coverage, quality, and temporal distribution of data spanning the past few Myr and the fact that zonal TAF models do not fit the observations, we investigate non-zonal TAF structure in the data. Differences between normal and reverse polarity data (Figure 8)

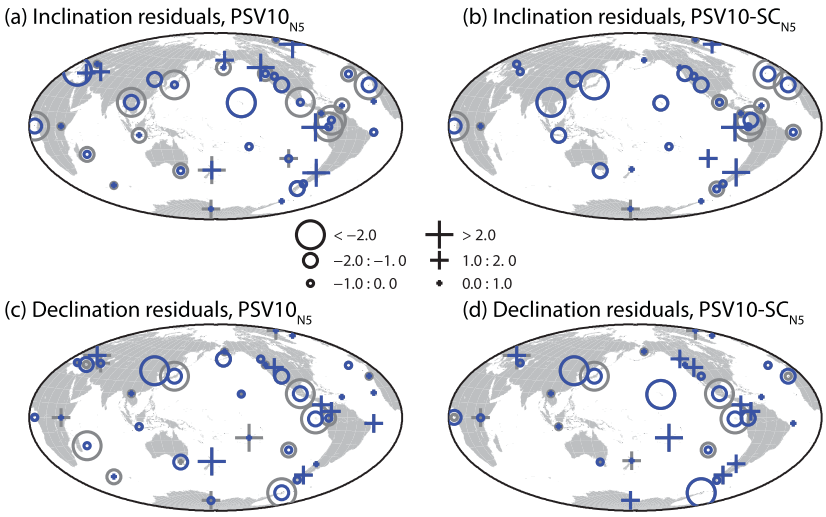

Figure 9. (a) Inclination and (c) declination residuals with respect to GAD (gray symbols) and non-zonal model LN3 (blue symbols) for the geographically binned 0–5 Ma normal polarity data set, PSV10$_{N5}$. Residuals are the time-averaged inclination or declination anomaly weighted by the uncertainty in the mean time-averaged field (TAF) direction at each location. (b) Inclination and (d) declination residuals with respect to GAD (gray) and non-zonal model LN3-SC (blue) for PSV10-SC$_{N5}$. The difference in size of the gray and blue symbols at a given location illustrates the change in misfit to the data from a GAD TAF model to the non-zonal TAF model. Locations at which only the blue symbol is visible have a change in misfit during the inversion that is less than the uncertainty in the TAF direction.

indicate that the two geomagnetic field states should be modeled independently; we focus on normal polarity data for the last 5 Myr as these comprise most of the sites (Figure 5b). Retaining only sites younger than 5 Ma also reduces any errors introduced by uncertainties in the already small plate motion corrections and allows comparison with previous non-zonal TAF studies based on the PSVRL data compilation (Gubbins & Kelly, 1993; Johnson & Constable, 1995, 1997; Kelly & Gubbins, 1997).

Geographic variations in departures from GAD in the 0–5 Ma normal polarity subset of PSV10 (hereafter PSV10$_{N5}$) are shown in Figures 9a and 9c. The TAF direction (unit vector mean) is computed for sites in 5°–10° geographical bins, based on the spatial distribution of data. The resulting time-averaged inclination and declination anomalies are normalized by the uncertainty in the mean direction (as in Johnson & Constable, 1995) to investigate the residual signal, i.e., the size of the TAF anomaly relative to the predicted field at a given location. Inclination residuals relative to GAD (Figure 9a) show dominantly large negative residuals at low latitudes but also regional variations.

Declination residuals (Figure 9c) show distinct regional variations, such as small residuals around the southwestern Pacific Ocean but large residuals in the south central Pacific Ocean and at low equatorial latitudes in the Americas. We also investigate the 0–5 Ma normal polarity subset of PSV10-SC, hereafter PSV10-SC$_{N5}$ (Figures 9b and 9d). As expected, the overall patterns of the PSV10-SC$_{N5}$ residuals are similar to those for PSV10$_{N5}$, but the signal can be different in locations where sequences of flows have been averaged in the PSV10-SC data set. For example, reduced inclination residual magnitudes are seen in western North America and Hawaii in PSV10-SC$_{N5}$, whereas the declination residual magnitude for Hawaii is significantly larger in PSV10-SC$_{N5}$ compared to PSV10$_{N5}$. This suggests distinct structure in the field at Hawaii, even in the PSV10-SC data set.

The regional structure in inclination and declination residuals suggests non-zonal TAF structure and we construct such models compatible with the data. We adopt the modeling approach of Johnson and Constable (1995, 1997) in which a low spherical harmonic degree and order TAF model is sought that includes both latitudinal and longitudinal structure, but that has minimal departure (see below) from a GAD description of the field. We generate models compatible with both PSV10$_{N5}$ and PSV10-SC$_{N5}$ to investigate any field structure that is required by PSV10$_{N5}$ but not by PSV10-SC$_{N5}$ and might thus be attributable to temporal oversampling at some locations. Below, we summarize the modeling approach (section 6.1) and show detailed

results from three inversions—two based on PSV10$_{N5}$ and one based on PSV10-SC$_{N5}$ (section 6.2). From these results, we propose two new 0–5 Ma TAF models: LN3 that fits PSV10$_{N5}$ and LN3-SC that fits PSV10-SC$_{N5}$. These are included in the supporting information. For LN3 and LN3-SC, we discuss geographical structure in the field at the core-mantle boundary, and in the inclination and declination anomalies predicted at Earth's surface. We compare LN3 and LN3-SC with previous 0–5 Myr normal polarity TAF models based on directional data from lava flows (e.g., LN1 and LN2 of Johnson and Constable (1995)) and with models for the Holocene field.

6.1. Inversion Approach

For a given inversion, regional TAF directions are computed in geographic bins (see above), and sites with transitional directions are excluded using the iterative Vandamme cutoff. As discussed earlier, even if it were possible to define precisely the percentage of time the field spends in a transitional state at all geographic locations, representative sampling of transitional directions in a lava flow data set is difficult to achieve in practice. Although the PSV10 data set contains a reasonable percentage of transitional directions overall (see section 3.3), at a regional level sampling of transitional directions is uneven and likely not representative of actual field behavior; thus, we do not include these sites in our non-zonal inversions. After binning, only regions with more than 10 sites are retained and we also investigate the effect of stricter criteria on the resulting models (see section 6.2). PSV10$_{N5}$ and PSV10-SC$_{N5}$ comprise data from 40 and 34 regions with, on average, 36 and 33 sites per region, respectively.

The TAF directions are inverted using the iterative nonlinear algorithm, Occam, (Constable et al., 1987; Johnson & Constable, 1995, 1997) to construct regularized field models. The regularization or smoothness constraint requires that models have minimum non-GAD structure, as well as fitting the observations to within a specified tolerance level, T. The chosen smoothness constraint minimizes the power in the non-GAD radial magnetic field at the core-mantle boundary (Johnson & Constable, 1995, 1997). The desired tolerance level is the 95% confidence limit on the expected value of the reduced chi-squared (χ^2), and the weighting matrix is computed from the standard error in the mean inclination and mean declination at each site as in Johnson and Constable (1997). We solved for models with a maximum spherical harmonic degree and order, l_{max}, of 10, and confirmed that the resulting models were not influenced by the cutoff in the spherical harmonic expansion (i.e., that models obtained using $l_{max} = 11$ were the same as those for $l_{max} = 10$).

6.2. Inversion Results

The results of a typical inversion are shown using the PSV10$_{N5}$ data set in Figure 10a. The starting model is GAD, which has a roughness of zero (no non-GAD power) and a weighted RMS misfit to the data of 2.05. The required tolerance, based on time-averaged D, I measurements for 40 regions, is $T = 1.31$. As the inversion proceeds, models with lower misfits and more structure (increasing model roughness) are found. Initially, relatively larger reductions in RMS misfit are found, but further decreases in RMS misfit can only be obtained at the expense of substantial increases in model roughness. Ideally, the preferred model is that obtained from the iteration at which the RMS misfit first meets the tolerance criterion. For PSV10$_{N5}$ this occurs at iteration 17 (Figure 10a, intersection of RMS misfit curve with dashed black line). However, later in the inversion, the increase in model roughness is not necessarily monotonic with iteration number. Pairs of iterations are seen where a relatively rough model at one iteration (e.g., iteration 17, Figure 10a) is followed by a smoother model at the next iteration (e.g., iteration 18, Figure 10a) that has a lower RMS misfit. This has been seen previously in Occam (see details in Johnson & Constable, 1997), and likely reflects inconsistent signals in the contributing data set. In Figure 10a, we show maps of the radial field B_r at the core-mantle boundary, CMB, for iteration 18 (the smoothest iteration that fits the data to within the specified tolerance limit) and for an earlier, smoother model (iteration 10) that has an RMS misfit of 1.58. The roughness for the model from iteration 18 is 3.7 versus a 0.9 for the model for iteration 10. Both models show non-zonal structure in B_r, with the model for iteration 18 showing considerably higher amplitude, shorter-spatial-scale structure as expected.

We investigated whether changing the required number of sites per region, or samples per site, affected the model results and produced more stable inversions. Tests showed that increasing the minimum number of sites per region from 10 to 20, i.e., requiring more sites for an "acceptable" time-average resulted in similar results to those shown in Figure 10a, i.e., the desired tolerance level was reached after the inversion started to become unstable. Increasing the minimum number of sites per region severely reduces the

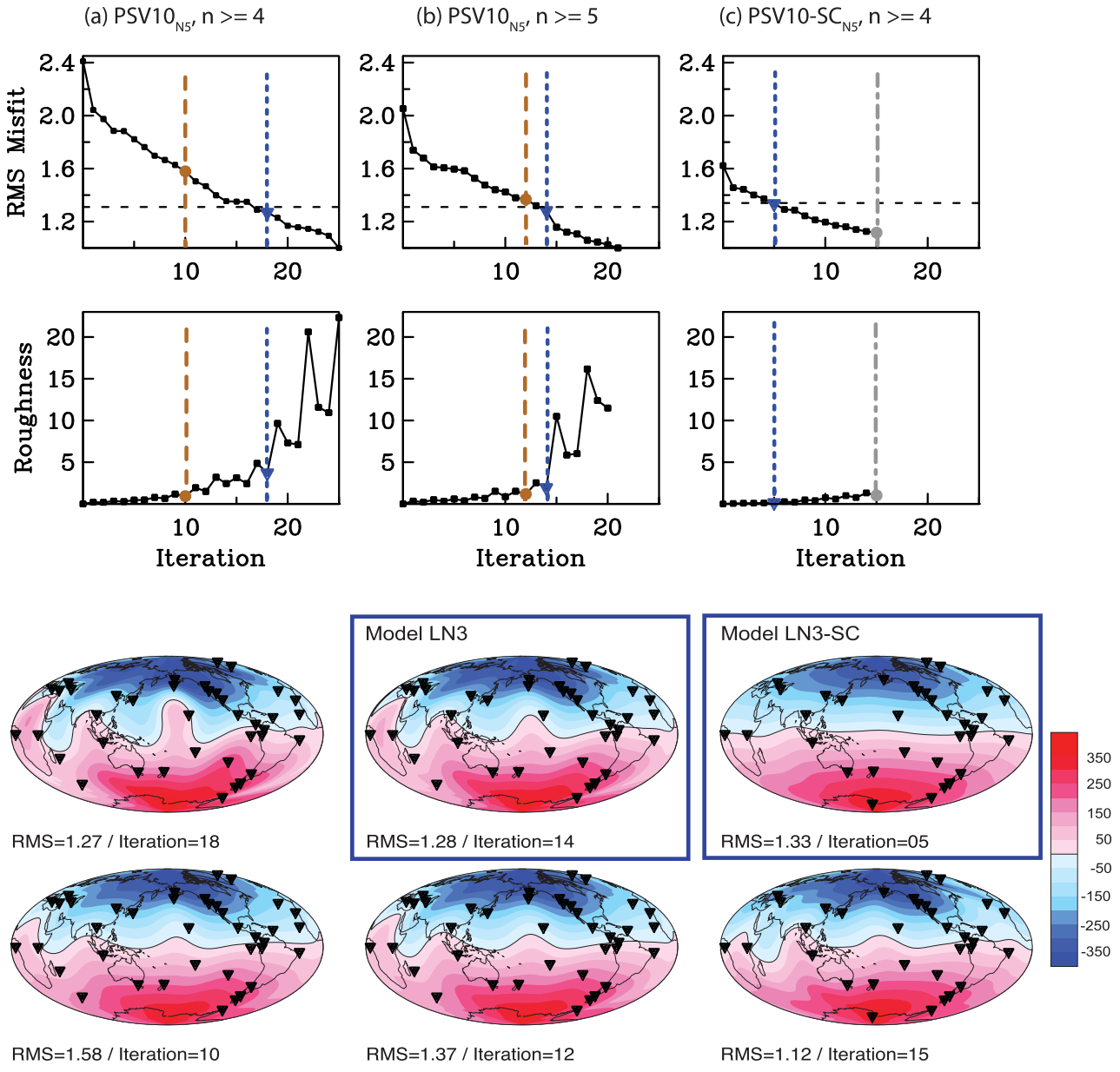

Figure 10. Results from inversions: (a, left column) the PSV10$_{N5}$ data set, retaining sites with at least $n \geq 4$ samples per site; (b, middle column) the PSV10$_{N5}$ data set, retaining sites with at least $n \geq 5$ samples per site; (c, right column) the PSV10-SC$_{N5}$ data set, retaining sites with $n \geq 4$. For each inversion the rows are as follows: (Row 1, top) Root-mean-square (RMS) misfit versus iteration number, with required tolerance shown as dashed black line; (Row 2) model roughness versus iteration number; (Row 3) *Br* at the core-mantel boundary (CMB) in μT for the smoothest model that fits the data to within the required tolerance (denoted by blue short dashed lines in Rows 1 and 2); and (Row 4) B_r at the CMB for another iteration in the inversion (denoted by brown or gray long dashed line in Rows 1 and 2, see text for details). Models LN3 and LN3-SC are indicated in the blue boxes.

number of regions for which a TAF direction is available, which in turn affects the inversion results: we therefore chose to keep our minimum 10 site requirement for each geographic region. We found that using only sites with at least five samples per site (instead of four) resulted in an inversion that remained stable until the iteration at which the tolerance level was reached (Figure 10b). B_r at the CMB is shown for the smoothest model with an RMS misfit less than T (i iteration 14) and for the last model before a notable jump in model roughness (iteration 12). The model for iteration 12 has an RMS misfit of 1.37, slightly greater than the required tolerance of $T = 1.31$. Structure in B_r at the CMB is very similar for these two models.

Examination of the 120 sites with $n = 4$ showed that some of these were occasional occurrences in studies in which most sites had $n \geq 5$, but some were sites from successive flows in large sections. Thus restricting our data to $n \geq 5$ effectively reduced the effects of serial correlation in a few studies. From here on, our discussion of non-zonal models for the PSV10$_{N5}$ data set refers to models produced using the $n \geq 5$ selection criteria, because of the better stability of this inversion (Figure 10b) compared to that for $n \geq 4$ (Figure 10a).

Inversion results from the PSV10-SC$_{N5}$ data set are shown in Figure 10c. Because the effects of serial correlation have already been addressed in this data set, we did not impose any additional data quality restriction and retained sites with $n \geq 4$. The inversion is stable until iteration 15, well after the required tolerance of $T = 1.34$ is reached at iteration 5. B_r at the CMB for the smoothest model that fits the data (iteration 5) has more muted structure than that required to fit the PSV10$_{N5}$ data set (iteration 14, Figure 10b). This is expected because of the temporal averaging inherent in the PSV10-SC$_{N5}$ data set and associated reduction in number of bins with more than 10 sites. We also show B_r at the CMB for iteration 15. The RMS misfit is 1.12 and the model has similar spatial structure to the models for PSV10-SC$_{N5}$ at iterations 12 and 14 (Figure 10b), supporting the notion that this level of structure is implied by the PSV10$_{N5}$ data.

6.3. Discussion

Fitting the observations to the required tolerance in LN3 and LN3-SC gives an overall reduction in the size of the residuals in Figure 9 although there are a few locations where the residuals increase due to mutually incompatible regional data. The detailed structure and amplitude in the models is sensitive to the linked effects of serial correlation and data distribution. Removing sites with possible serial correlation affects the data distribution, eliminating coverage in some geographical bins because of a reduction in the number of sites in the region to less than 10. As a result, the overall non-zonal signal in B_r at the CMB is smaller for LN3-SC than LN3 (Figure 10c versus Figure 10b). Predictions from LN3 and LN3-SC provide inclination anomalies (ΔI, Figures 11a and 11b) and declination anomalies (ΔD, Figures 12a and 12b) relative to GAD at Earth's surface.

The dominant non-GAD term for LN3 is the axial quadrupole g_2^0 which produces an overall north-south hemispheric asymmetry in the field, and overall negative inclination anomalies at low latitudes (Figure 11a). The g_2^0 term is 3.0% of g_1^0, which is not sufficiently large to produce detectable north-south asymmetries in VGP dispersion. LN3, and all models for PSV10$_{N5}$ using at least five samples per site, show longitudinal variations in the magnetic equator and regions of increased radial flux at high latitudes over the Americas, the Indian Ocean and Asia. ΔI and ΔD at the surface also exhibit substantial variations in longitude, highlighting the need for this structure to explain the observations.

Model LN3 can be seen as a direct successor to LN1, and other 0–5 Myr models based on directions from lava flows (Gubbins & Kelly, 1993; Johnson & Constable, 1995; Kelly & Gubbins, 1997). There are similarities

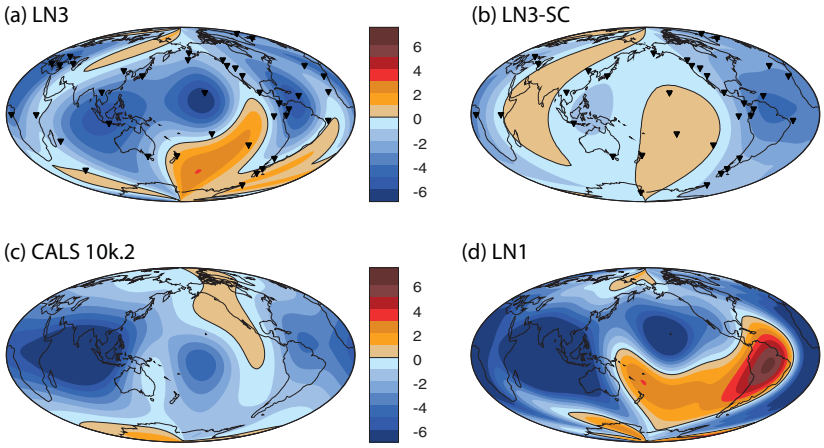

Figure 11. Inclination anomalies, ΔI at the Earth's surface in degrees predicted by models (a) LN3, (b) LN3-SC, (c) CALS10k.2 (Constable et al., 2016), and (d) LN1 (Johnson & Constable, 1995). Contour intervals are 1°.

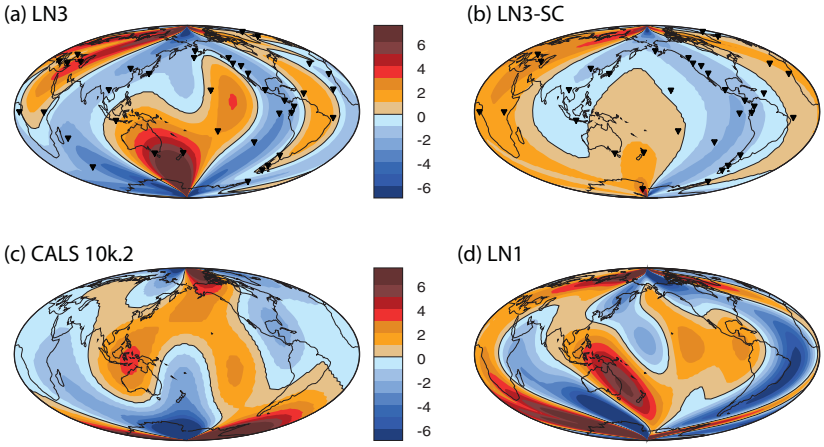

Figure 12. Declination anomalies, ΔD at the Earth's surface in degrees predicted by models (a) LN3, (b) LN3-SC, (c) CALS10k.2 (Constable et al., 2016), and (d) LN1 (Johnson & Constable, 1995). Contour intervals are 1°.

in the morphology of ΔI for LN3 and LN1 (Figures 11a and 11d, respectively), but the overall amplitude is considerably reduced in LN3, as a result of the substantial improvement in data coverage and quality afforded by the $PSV10_{N5}$ data set. The one region where ΔI predicted by LN3 and LN1 is quite different is South America. LN3 predicts negative inclinations, consistent with other low latitude sites, in contrast to a large positive inclination predicted by LN1. ΔD for LN3 and LN1 (Figures 12a and 12d) also differ most over the Americas and the Atlantic. These differences in ΔD and ΔI reflect the greatly enhanced data distribution over the Americas in PSV10 compared with earlier paleodirectional data compilations. The axial quadrupole g_2^0 is also the dominant term during the Holocene period as can be seen in ΔI for Model CALS10k.2 (Constable et al., 2016) in Figure 11c. LN3 shows some differences in non-zonal structure c.f. CALS10k.2. In particular the strong Indian Ocean negative ΔI and weak positive ΔI over western North America and the northwest Pacific in CALS10k.2 are not seen in LN3. This suggests that more than 10 kyr is needed to fully recover stable structure in the basic field morphology.

Finally, model LN3-SC is more muted in structure, in particular in non-zonal structure, than model LN3. As described above this reflects the removal of possibly serially correlated sites, but equally importantly the reduction in geographical coverage that results from this. For example, PSV10-SC lacks key Southern Hemisphere coverage in the Indian Ocean relative to its PSV10 counterpart. Figures 11 and 12 show correspondingly weaker ΔI and ΔD at the surface with substantial differences in structure from LN3, despite qualitatively similar, albeit damped, structure in *Br* at the CMB. As discussed in section 6.2, inversions using PSV10-SC are in fact stable to lower RMS misfits than that corresponding to LN3-SC and models for those lower misfits (e.g., iteration 15 of the PSV10-SC data set in Figure 10c) are very similar to LN3. Thus, we consider LN3-SC a conservative end-member for structure in the normal polarity 0–5 Ma TAF.

7. Conclusions

We have compiled a new data set, PSV10, of high-quality paleodirectional results from lava flows that includes 2,401 sites from 81 studies published between 1989 and 2017. Paleomagnetic data from all studies can be found in the MagIC database (https://earthref.org/MAGIC). PSV10 comprises a five-fold increase in high-quality data over the PSVRL data base (McElhinny & McFadden, 1997), with greatly improved spatial coverage, particularly in the Southern Hemisphere. Temporal sampling is substantially improved at many locations, as is temporal control in the data set, with ~40% of sites in PSV10 having associated radiometric or historic ages. We addressed the issue of temporal oversampling by sequences of lava flows extruded over short time scales using two approaches: either averaging the directional information from all flows in a given section, or retaining only the top and bottom flows. The resulting derived data sets are denoted by PSV10-SC and PSV10-TB, respectively.

Paleodirectional data from Hawaii have often been interpreted to show a large departure from GAD in the time-averaged field (e.g., Johnson & Constable, 1997) and low PSV (e.g., Doell & Cox, 1963). In PSV10, the extensive data set from Hawaii comprises data from several distinct lava flow sections that may result in oversampling of limited time intervals, with associated biased estimates of PSV. The effects of such oversampling are reduced in PSV10-SC (to the effect possible given the sections sampled): this data set shows a reduced magnitude inclination anomaly, but somewhat surprisingly, a larger declination anomaly than in PSV10.

We analyzed latitudinal variations in PSV and the TAF. A new feature in this compilation is the substantially larger increase in S_F with latitude in the Southern Hemisphere than in the north, an asymmetry noted by Cromwell et al. (2013a), and well documented for the Holocene time interval (Constable et al., 2016). This asymmetry is not present when the Vandamme VGP cutoff criterion is applied, suggesting that it reflects geographical differences in the percentage of transitional sites. PSV10 and PSV10-SC show some general agreement with values predicted by Model G and TK03. However, neither data set is statistically fit by either model for PSV or by GAD or simple zonal variations in the non-GAD field for the TAF.

We used normal polarity sites for 0–5 Ma from PSV10 and PSV10-SC to generate new regularized TAF models that allow non-zonal structure. The resulting models, LN3 and LN3-SC show non-zonal structure, with LN3-SC showing more muted structure than LN3 as a result of the correction for serial correlation and the reduced data coverage. LN3 shows similarities to previous 0–5 Ma non-zonal TAF models (Gubbins & Kelly, 1993; Johnson & Constable, 1995; Kelly & Gubbins, 1997), in particular longitudinal variations in the magnetic equator and regions of increased radial flux at high latitudes over the Americas, the Indian Ocean and Asia. These models constitute the first global TAF models made from a global data set that meets modern laboratory protocols and that has greatly improved geographical coverage over previous data compilations.

Acknowledgments
We thank the MagIC database team (Anthony Koppers, Rupert Minnett, and Ron Shaar) for supporting the data preservation efforts of this manuscript. Thanks to Hubert Staudigel, Jeff Gee, Tom Levy, Andy Biggin, Anita Di Chiara, and Florian Lhuillier for their constructive reviews. This material is based on work supported in part by National Science Foundation grants EAR1141840, EAR1345003, and PLR1541285 to L.T., EAR1246826 and EAR1623786 to C.G.C., and the Natural Sciences and Engineering Research Council of Canada to C.L.J. Data for the PSV10, PSV10-SC, and PSV10-TB compilations can be found in the MagIC online data repository at https://earthref.org/MagIC/DOI/10.1002/2017GC007318. Gauss coefficients for TAF model LN3 and LN3-SC can be found at https://earthref.org/ERDA/2221/ and https://earthref.org/ERDA/2222/, respectively, in the EarthRef Digital Archive. PSV10, PSV10-SC, and PSV10-TB and the TAF models LN3 and LN3-SC are also provided as files in the supporting information.

References

Alva-Valdivia, L. M. (2005). Comprehensive paleomagnetic study of a succession of Holocene olivine-basalt flow: Xitle Volcano (Mexico) revisited. *Earth, Planets and Space*, *57*(9), 839–853. https://doi.org/10.1186/BF03351862

Alva-Valdivia, L. M., Goguitchaichvili, A., & Urrutia-Fucugauchi, J. (2001). Further constraints for the Plio-Pleistocene geomagnetic field strength: New results from the Los Tuxtlas volcanic field. *Earth, Planets and Space*, *53*(9), 873–881. https://doi.org/10.1186/BF03351684

Argus, D. F., Gordon, R. G., & DeMets, C. (2011). Geologically current motion of 56 plates relative to the no-net-rotation reference frame. *Geochemistry, Geophysics, Geosystems*, *12*, Q11001. https://doi.org/10.1029/2011GC003751

Baraldo, A., Rapalini, A. E., Böhnel, H., & Mena, M. (2003). Paleomagnetic study of Deception Island, South Shetland Islands, Antarctica. *Geophysical Journal International*, *153*(2), 333–343. https://doi.org/10.1046/j.1365-246X.2003.01881.x

Brassart, J., Tric, E., Valet, J. P., & Herrero-Bervera, E. (1997). Absolute paleointensity between 60 and 400 ka from the Kohala Mountain (Hawaii). *Earth and Planetary Science Letters*, *148*(1–2), 141–156. https://doi.org/10.1016/S0012-821X(97)00024-1

Brown, L. L., Singer, B. S., & Gorring, M. L. (2004). Paleomagnetism and $^{40}Ar/^{39}Ar$ chronology of lavas from Meseta del Lago Buenos Aires, Patagonia. *Geochemistry, Geophysics, Geosystems*, *5*, Q01H04. https://doi.org/10.1029/2003GC000526

Brown, M. C., Singer, B. S., Knudsen, M. F., Jicha, B. R., Finnes, E., & Feinberg, J. M. (2009). No evidence for Brunhes age excursions, Santo Antão, Cape Verde. *Earth and Planetary Science Letters*, *287*(1–2), 100–115. https://doi.org/10.1016/j.epsl.2009.07.039

Calvo-Rathert, M., Aguilar Reyes, B., Goguitchaichvili, A., Rosas Elguera, J., Franco, H., Morales, J., et al. (2013). Rock-magnetic and paleomagnetic results from the Tepic-Zacoalco rift region (Western Mexico). *Studia Geophysica et Geodaetica*, *57*(2), 309–331. https://doi.org/10.1007/s11200-012-0239-y

Calvo-Rathert, M., Bógalo, M. F., Gogichaishvili, A., Sologashvili, J., & Vashakidze, G. (2013). New paleomagnetic and paleointensity data from Pliocene lava flows from the Lesser Caucasus. *Journal of Asian Earth Sciences*, *73*, 347–361. https://doi.org/10.1016/j.jseaes.2013.04.039

Calvo-Rathert, M., Goguitchaichvili, A., Bógalo, M.-F., Vegas-Tubía, N., Carrancho, A., & Sologashvili, J. (2011). A paleomagnetic and paleointensity study on Pleistocene and Pliocene basaltic flows from the Djavakheti Highland (Southern Georgia, Caucasus). *Physics of the Earth and Planetary Interiors*, *187*(3–4), 212–224. https://doi.org/10.1016/j.pepi.2011.03.008

Calvo-Rathert, M., Goguitchaichvili, A., & Vegas-Tubia, N. (2009). A paleointensity study on Middle Miocene to Pliocene volcanic rocks from south-eastern Spain. *Earth, Planets and Space*, *61*(1), 61–69. https://doi.org/10.1186/BF03352885

Camps, P., Henry, B., Prevot, M., & Faynot, L. (2001). Geomagnetic paleosecular variation recorded in Plio-Pleistocene volcanic rocks from Possession Island (Crozet Archipelago, southern Indian Ocean). *Journal of Geophysical Research*, *106*(B2), 1961–1971. https://doi.org/10.1029/2000JB900370

Cande, S. C., & Kent, D. V. (1995). Revised calibration of the geomagnetic polarity timescale for the Late Cretaceous and Cenozoic. *Journal of Geophysical Research*, *100*(B4), 6093–6095. https://doi.org/10.1029/94JB03098

Canon-Tapia, E., Herrero-Bervera, E., & Walker, G. P. L. (1994). Flow directions and paleomagnetic study of rocks from the Azufre volcano Argentina. *Journal of Geomagnetism and Geoelectricity*, *46*(2), 143–159.

Carlut, J., Quidelleur, X., Courtillot, V., & Boudon, G. (2000). Paleomagnetic directions and K/Ar dating of 0 to 1 Ma lava flows from La Guadeloupe Island (French West Indies): Implications for time-averaged field models. *Journal of Geophysical Research*, *105*(B1), 835–849. https://doi.org/10.1029/1999JB900238

Ceja, M. R., Goguitchaichvili, A., Calvo-Rathert, M., Morales-Contreras, J., Alva-Valdivia, L., Elguera, J., et al. (2006). Paleomagnetism of the Pleistocene Tequila Volcanic Field (Western Mexico). *Earth, Planets and Space*, *58*(10), 1349–1358. https://doi.org/10.1186/BF03352631

Chauvin, A., Gillot, P. Y., & Bonhommet, N. (1991). Paleointensity of the Earth's magnetic field recorded by two late Quaternary volcanic sequences at the Island of La Réunion (Indian Ocean). *Journal of Geophysical Research*, *96*(B2), 1981–2006. https://doi.org/10.1029/90JB02223

Clement, B. M. (2004). Dependence of the duration of geomagnetic polarity reversals on site latitude. *Nature*, *428*(6983), 637–640. https://doi.org/10.1038/nature02459

Coe, R. S., Zhao, X., Lyons, J., Pluhar, C., & Mankinen, E. (2000). Revisiting the 1964 collection of Nunivak lava flows. *Eos, Transactions American Geophysical Union*, *81*(48), Fall Meeting Suppl., Abstract GP62A-06.

Constable, C. G., & Johnson, C. L. (1999). Anisotropic paleosecular variation models: Implications for geomagnetic field observables. *Physics of the Earth and Planetary Interiors*, *115*(1), 35–51. https://doi.org/10.1016/S0031-9201(99)00065-5

Constable, C. G., Korte, M., & Panovska, S. (2016). Persistent high paleosecular variation activity in Southern Hemisphere for at least 10,000 years. *Earth and Planetary Science Letters*, *453*, 78–86. https://doi.org/10.1016/j.epsl.2016.08.015

Constable, C. G., & Parker, R. L. (1988). Statistics of the geomagnetic secular variation for the past 5 m.y. *Journal of Geophysical Research*, *93*(B10), 11569–11581. https://doi.org/10.1029/JB093iB10p11569

Constable, S. C., Parker, R. L., & Constable, C. G. (1987). Occam's inversion: A practical algorithm for generating smooth models from electromagnetic sounding data. *Geophysics*, *52*(3), 289–300. https://doi.org/10.1190/1.1442303

Conte-Fasano, G., Urrutia-Fucugauchi, J., Goguitchaichvili, A., & Morales-Contreras, J. (2006). Low-latitude paleosecular variation and the time-averaged field during the Late Pliocene and Quaternary-paleomagnetic study of the Michoacan-Guanajuato volcanic field, Central Mexico. *Earth, Planets and Space*, *58*(10), 1359–1371. https://doi.org/10.1186/BF03352632

Creer, K. M. (1983). Computer synthesis of geomagnetic palaeosecular variations. *Nature*, *304*(5928), 695–699. https://doi.org/10.1038/304695a0

Cromwell, G., Constable, C. G., Staudigel, H., Tauxe, L., & Gans, P. B. (2013). Revised and updated paleomagnetic results from Costa Rica. *Geochemistry Geophysics Geosystems*, *14*, 3379–3388. https://doi.org/10.1002/ggge.20199

Cromwell, G., Tauxe, L., Staudigel, H., Constable, C. G., Koppers, A. A. P., & Pedersen, R.-B. (2013). In search of long term hemispheric asymmetry in the geomagnetic field: Results from high northern latitudes. *Geochemistry Geophysics Geosystems*, *14*, 3234–3249. https://doi.org/10.1002/ggge.20174

Davies, C. J., & Constable, C. G. (2014). Insights from geodynamo simulations into long-term geomagnetic field behaviour. *Earth and Planetary Science Letters*, *404*, 238–249. https://doi.org/10.1016/j.epsl.2014.07.042

Di Chiara, A., Speranza, F., Porreca, M., Pimentel, A., D'Ajello Caracciolo, F., & Pacheco, J. (2014). Constraining chronology and time-space evolution of Holocene volcanic activity on the Capelo Peninsula (Faial Island, Azores): The paleomagnetic contribution. *Geological Society of America Bulletin*, *126*(9–10), 1164–1180. https://doi.org/10.1130/B30933.1

Doell, R. R., & Cox, A. (1963). The accuracy of the paleomagnetic method as evaluated from historic Hawaiian lava flows. *Journal of Geophysical Research*, *68*(7), 1997–2009. https://doi.org/10.1029/JZ068i007p01997

Dominguez, A. R., & Van der Voo, R. (2014). Secular variation of the Middle and Late Miocene geomagnetic field recorded by the Columbia River basalt group in Oregon, Idaho and Washington, USA. *Geophysical Journal International*, *197*(3), 1299–1320. https://doi.org/10.1093/gji/ggt487

Donadini, F., Korte, M., & Constable, C. G. (2009). Geomagnetic field for 0–3 ka: 1. New data sets for global modeling. *Geochemistry Geophysics Geosystems*, *10*, Q06007. https://doi.org/10.1029/2008GC002295

Døssing, A., Muxworthy, A. R., Supakulopas, R., Riishuus, M. S., & Mac Niocaill, C. (2016). High northern geomagnetic field behavior and new constraints on the Gilsá event: Paleomagnetic and $^{40}Ar/^{39}Ar$ results of ~0.5–3.1 Ma basalts from Jökuldalur, Iceland. *Earth and Planetary Science Letters*, *456*, 98–111. https://doi.org/10.1016/j.epsl.2016.09.022

Elmaleh, A., Valet, J.-P., Quidelleur, X., Solihin, A., Bouquerel, H., Tesson, T., et al. (2004). Palaeosecular variation in Java and Bawean Islands (Indonesia) during the Brunhes Chron. *Geophysical Journal International*, *157*(1), 441–454. https://doi.org/10.1111/j.1365-246X.2004.02197.x

Fisher, R. A. (1953). Dispersion on a sphere. *Proceedings of the Royal Society of London. Series A*, *217*(1130), 295–305. https://doi.org/10.1098/rspa.1953.0064

Goguitchaichvili, A., Alva-Valdivia, L., Rosas-Elguera, J., Urrutia-Fucugauchi, J., Cervantes, M., & Morales, J. (2002). Paleosecular variation record of the geomagnetic full vector during Late Miocene, from the Nayarit Area, Mexico. *Physics of the Earth and Planetary Interiors*, *134*(1–2), 71–88. https://doi.org/10.1016/S0031-9201(02)00096-1

Goguitchaichvili, A., Calvo, M., Sologashvili, D., Alva, L., & Urrutia, J. (2000). Paleomagnetism of Georgian Plio-Quaternary volcanic provinces (Southern Caucasus): A pilot study. *Comptes Rendus de l'Academie des Sciences, Seris IIa: Sciences de la Terre et des Planetes*, *331*(11), 683–690. https://doi.org/10.1016/S1251-8050(00)01471-3

Goguitchaichvili, A., Gonzalez, J., Pluhar, C., Alva-Valdivia, L., Rosas-Elguera, J., Ruiz-Martinez, V., et al. (2011). A comprehensive rock-magnetic, paleomagnetic, paleointensity and geochronologic study along the Western Trans-Mexican volcanic belt: Geodynamic and geomagnetic implications. *Geofisica Internacional*, *50*(2), 227–254.

Goguitchaichvili, A., Petronille, M., Henry, B., Alva-Valdivia, L., Morales, J., & Urrutia-Fucugauchi, J. (2007). Paleomagnetism of the Eastern Alkaline Province (Mexico): Contribution to the time-averaged field global database and geomagnetic instability time scale. *Earth, Planets and Space*, *59*(7), 775–783. https://doi.org/10.1186/BF03352740

Gonzalez, S., Sherwood, G., Böhnel, H., & Schnepp, E. (1997). Palaeosecular variation in Central Mexico over the last 30,000 years: The record from lava flows. *Geophysical Journal International*, *130*(1), 201–219. https://doi.org/10.1111/j.1365-246X.1997.tb00999.x

Gubbins, D., & Kelly, P. (1993). Persistent patterns in the geomagnetic field over the past 2.5 myr. *Nature*, *365*(6449), 829–832. https://doi.org/10.1038/365829a0

Hagstrum, J. T., Fleck, R. J., Evarts, R. C., & Calvert, A. T. (2017). Paleomagnetism and $^{40}Ar/^{39}Ar$ geochronology of the Plio-Pleistocene Boring Volcanic Field: Implications for the geomagnetic polarity time scale and paleosecular variation. *Physics of the Earth and Planetary Interiors*, *262*, 101–115. https://doi.org/10.1016/j.pepi.2016.07.008

Herrero-Bervera, E., Margas-Vinuela, J., & Valet, J.-P. (2000). Paleomagnetic study of the ages of lavas on the island of Lanaï, Hawaï`i. *Journal of Volcanology and Geothermal Research*, *104*(1–4), 21–31. https://doi.org/10.1016/S0377-0273(00)00197-9

Herrero-Bervera, E., & Valet, J.-P. (2002). Paleomagnetic secular variation of the Honolulu volcanic series (33–700 ka), O'ahu (Hawaii). *Physics of the Earth and Planetary Interiors*, *133*(1–4), 83–97. https://doi.org/10.1016/S0031-9201(02)00092-4

Herrero-Bervera, E., & Valet, J.-P. (2003). Persistent anomalous inclinations recorded in the Koolau volcanic series on the Island of Oahu (Hawaii, USA) between 1.8 and 2.6 Ma. *Earth and Planetary Science Letters*, *212*(3–4), 443–456. https://doi.org/10.1016/S0012-821X(03)00168-7

Herrero-Bervera, E., & Valet, J. P. (2007). Holocene paleosecular variation from dated lava flows on Maui (Hawaii). *Physics of the Earth and Planetary Interiors*, *161*(3–4), 267–280. https://doi.org/10.1016/j.pepi.2007.02.008

Johnson, C. L., & Constable, C. G. (1997). The time-averaged geomagnetic field: Global and regional biases for 0–5 Ma. *Geophysical Journal International*, *131*(3), 643–666. https://doi.org/10.1111/j.1365-246X.1997.tb06604.x

Johnson, C. L., & Constable, C. G. (1996). Palaeosecular variation recorded by lava flows over the past five million years. *Philosophical transactions of the Royal Society of London. Series A*, *354*(1704), 89–141. https://doi.org/10.1098/rsta.1996.0004
Johnson, C. L., & Constable, C. G. (1995). The time-averaged geomagnetic field as recorded by lava flows over the last 5 Myr. *Geophysical Journal International*, *122*(2), 489–519. https://doi.org/10.1111/j.1365-246X.1995.tb07010.x
Johnson, C. L., Wijbrans, J. R., Constable, C. G., Gee, J., Staudigel, H., Tauxe, L., et al. (1998). Ar-40/Ar-39 ages and paleomagnetism of Sao Miguel lavas, Azores. *Earth and Planetary Science Letters*, *160*, 637–649. https://doi.org/10.1016/S0012-821X(98)00117-4
Johnson, C. L., Constable, C. G., Tauxe, L., Barendregt, R., Brown, L. L., Coe, R. S., et al. (2008). Recent investigations of the 0–5 Ma geomagnetic field recorded by lava flows. *Geochemistry, Geophysics, Geosystems*, *9*, Q04032. https://doi.org/10.1029/2007GC001696
Johnson, C. L., & McFadden, P. L. (2015). The time-averaged field and paleosecular variation. In Kono, M. (Ed.), *Geomagnetism*; Schubert, G. (Ed.), *Treatise on geophysics* (2nd ed., Vol. 5, pp. 385–417). Amsterdam, The Netherlands: Elsevier. https://10.1016/B978-0-444-53802-4.00105-6
Kelly, P., & Gubbins, D. (1997). The geomagnetic field over the past 5 million years. *Geophysical Journal International*, *128*(2), 315–330. https://doi.org/10.1111/j.1365-246X.1997.tb01557.x
Kent, D. V., Wang, H., & Rochette, P. (2010). Equatorial paleosecular variation of the geomagnetic field from 0–3 ma lavas from the Galapagos Islands. *Physics of the Earth and Planetary Interiors*, *183*(3–4), 404–412. https://doi.org/10.1016/j.pepi.2010.08.010
Khokhlov, A., & Hulot, G. (2013). Probability uniformization and application to statistical palaeomagnetic field models and directional data. *Geophysical Journal International*, *193*(1), 110–121. https://doi.org/10.1093/gji/ggs118
Kissel, K., Rodriguez-Gonzalez, A., Laj, C., Perez-Torrado, F., Carracedo, J. C., Wandres, C., et al. (2015). Paleosecular variation of the earth magnetic field at the Canary Islands over the last 15 ka. *Earth and Planetary Science Letters*, *412*, 52–60. https://doi.org/10.1016/j.epsl.2014.12.031
Kono, M., & Tanaka, H. (1995). Mapping the gauss coefficients to the pole and the models of paleosecular variation. *Journal of Geomagnetism and Geoelectricity*, *47*(1), 115–130. https://doi.org/10.5636/jgg.47.115
Laj, C., Guillou, H., Szeremeta, N., & Coe, R. (1999) Geomagnetic paleosecular variation at Hawaii around 3 Ma from a sequence of 107 lava flows at Kaena Point (Oahu). *Earth and Planetary Science Letters*, *170*(4), 365–376. https://doi.org/10.1016/S0012-821X(99)00119-3
Laj, C., Rais, A., Surmont, J., Gillot, P.-Y., Guillou, H., Kissel, C., et al. (1997). Changes of the geomagnetic field vector obtained from lava sequences on the Island of Vulcano (Aeolian Islands, Sicily). *Physics of the Earth and Planetary Interiors*, *99*(3–4), 161–177. https://doi.org/10.1016/S0031-9201(96)03221-9
Lawrence, K. P., Constable, C. G., & Johnson, C. L. (2006). Paleosecular variation and the average geomagnetic field at +/–20 degrees latitude. *Geochemistry Geophysics Geosystems*, *7*, Q07007. https://doi.org/10.1029/2005GC001181
Lawrence, K. P., Tauxe, L., Staudigel, H., Constable, C. G., Koppers, A. A. P., McIntosh, W. C., et al. (2009). Paleomagnetic field properties at high southern latitude. *Geochemistry, Geophysics, Geosystems*, *10*, Q01005. https://doi.org/10.1029/2008GC002072
Lee, S. (1983). *A study of the time-averaged paleomagnetic field for the past 195 million years* (PhD thesis). Canberra, ACT, Australia: Australian National University.
Leonhardt, R., Matzka, J., & Menor, E. A. (2003). Absolute paleointensities and paleodirections of Miocene and Pliocene lavas from Fernando de Noronha, Brazil. *Physics of the Earth and Planetary Interiors*, *139*(3–4), 285–303. https://doi.org/10.1016/j.pepi.2003.09.008
Leonhardt, R., & Soffel, H. C. (2006). The growth, collapse and quiescence of Teno volcano, Tenerife: new constraints from paleomagnetic data. *International Journal of Earth Science*, *95*, 1053–1064. https://doi.org/10.1007/s00531-006-0089-3
Lhuillier, F., & Gilder, S. A. (2013). Quantifying paleosecular variation: Insights from numerical dynamo simulations. *Earth and Planetary Science Letters*, *382*, 87–97. https://doi.org/10.1016/j.epsl.2013.08.048
Lhuillier, F., Shcherbakov, V. P., Gilder, S. A., & Hagstrum, J. T. (2017). Variability of the 0-3 Ma palaeomagnetic field observed from the Boring Volcanic Field of the Pacific Northwest. *Geophysical Journal International*, *211*(1), 69–79. https://doi.org/10.1093/gji/ggx288
Lowes, F. J. (1974). Spatial power spectrum of the main geomagnetic field, and extrapolation to the core. *Geophysical Journal International*, *36*(3), 717–730. https://doi.org/10.1111/j.1365-246X.1974.tb00622.x
Mankinen, E. A., & Cox, A. (1988). Paleomagnetic investigation of some volcanic-rocks from the McMurdo Volcanic Province, Antarctica. *Journal of Geophysical Research*, *93*(B10), 11599–11612. https://doi.org/10.1029/JB093iB10p11599
McElhinny, M. W., & McFadden, P. L. (1997). Palaeosecular variation over the past 5 Myr based on a new generalized database. *Geophysical Journal International*, *131*(2), 240–252. https://doi.org/10.1111/j.1365-246X.1997.tb01219.x
McElhinny, M. W., & McFadden, P. L. (2000). *Paleomagnetism: Continents and Oceans* (2nd ed., 386 pp.). San Diego, CA: Academic Press.
McElhinny, M. W., McFadden, P. L., & Merrill, R. T. (1996). The time-averaged paleomagnetic field 0–5 Ma. *Journal of Geophysical Research*, *101*(B11), 25007–25027. https://doi.org/10.1029/96JB01911
McElhinny, M. W., & Merrill, R. T. (1975). Geomagnetic secular variation over the past 5 m.y. *Reviews of Geophysics and Space Physics*, *13*(5), 687–708. https://doi.org/10.1029/RG013i005p00687
McFadden, P. L., Merrill, R. T., & McElhinny, M. W. (1988). Dipole/quadrupole family modeling of paleosecular variation. *Journal of Geophysical Research*, *93*(B10), 11583–11588. https://doi.org/10.1029/JB093iB10p11583
Mejia, V., Barendregt, R. W., & Opdyke, N. D. (2002). Paleosecular variation of Brunhes age lava flows from British Columbia, Canada. *Geochemistry, Geophysics, Geosystems*, *3*(12), 8801. https://doi.org/10.1029/2002GC000353
Mejia, V., Böhnel, H., Opdyke, N. D., Ortega-Rivera, M. A., Lee, J. K. W., & Aranda-Gomez, J. J. (2005). Paleosecular variation and time-averaged field recorded in late Piocene–Holocene lava flows from Mexico. *Geochemistry Geophysics Geosystems*, *6*, Q07H19. https://doi.org/10.1029/2004GC000871
Mejia, V., Opdyke, N. D., Vilas, J. F., Singer, B. S., & Stoner, J. S. (2004). Plio-Pleistocene time-averaged field in southern Patagonia recorded in lava flows. *Geochemistry, Geophysics, Geosystems*, *5*, Q03H08. https://doi.org/10.1029/2003GC000633
Merrill, R. T., & McElhinny, M. W. (1977). Anomalies in time-averaged paleomagnetic field and their implications for the lower mantle. *Reviews of Geophysics and Space Physics*, *15*(3), 309–323. https://doi.org/10.1029/RG015i003p00309
Merrill, R. T., McElhinny, M. W., & McFadden, P. L. (1996). *The magnetic field of the Earth: Paleomagnetism, the Core, and the Deep Mantle* (2nd ed., 531 pp.). San Diego, CA: Academic Press.
Michalk, D. M., Böhnel, H. N., Nowaczyk, N. R., Aguírre-Diaz, G. J., López-Martínez, M., Ownby, S., et al. (2013). Evidence for geomagnetic excursions recorded in Brunhes and Matuyama Chron lavas from the trans-Mexican volcanic belt. *Journal of Geophysical Research: Solid Earth*, *118*, 2648–2669. https://doi.org/10.1002/jgrb.50214
Miki, M., Inokuchi, S., Yamaguchi, S., Matsuda, J., Nagao, N., Isezaki, N., et al. (1998). Geomagnetic paleosecular variation in Easter Island, the Southeast Pacific. *Physics of the Earth and Planetary Interiors*, *129*, 205–243. https://doi.org/10.1016/S0031-9201(97)00106-4
Mitchell, R. J., Jaeger, D. J., Diehl, J. F., & Hammond, P. E. (1989). Paleomagnetic results from the Indian Heaven volcanic field, south-central Washington. *Geophysical Journal*, *97*(3), 381–390. https://doi.org/10.1111/j.1365-246X.1989.tb00509.x

Morales, J., Goguitchaichvili, A., Canon-Tapia, E., & Negrete, R. (2003). Further absolute geomagnetic paleointensities from Baja California: Evaluation of Pliocene and Early/Middle Pleistocene data. *Comptes Rendus Geoscience*, *335*(14), 995–1004. https://doi.org/10.1016/j.crte.2003.07.002

Morales, J., Goguitchaichvili, A., & Urrutia-Fucugauchi, J. (2001). A rock-magnetic and paleointensity study of some Mexican volcanic lava flows during the latest Pleistocene to the Holocene. *Earth, Planets and Space*, *53*(9), 893–902. https://doi.org/10.1186/BF03351686

Oliva-Urcia, B., Gil-Peña, I., Maestro, A., López-Mártinez, J., Galindo-Zaldívar, J., Soto, R., et al. (2016). Paleomagnetism from Deception Island (South Shetlands Archipelago, Antarctica), new insights into the interpretation of the volcanic evolution using a geomagnetic model. *International Journal of Earth Sciences*, *105*(5), 1353–1370. https://doi.org/10.1007/s00531-015-1254-3

Opdyke, N. D., Hall, M., Mejia, V., Huang, K., & Foster, D. A. (2006). Time-averaged field at the equator: Results from Ecuador. *Geochemistry, Geophysics, Geosystems*, *7*, Q11005. https://doi.org/10.1029/2005GC001221

Opdyke, N. D., Kent, D. V., Foster, D., & Huang, K. (2015). Paleomagnetism of Miocene volcanics on Sao Tome: Paleosecular variation at the equator and a comparison to its latitudinal dependence over the last 5 Myr. *Geochemistry, Geophysics, Geosystems*, *16*, 3870–3882. https://doi.org/10.1002/2015GC005901

Opdyke, N. D., Kent, D. V., Huang, K., Foster, D. A., & Patel, J. P. (2010). Equatorial paleomagnetic time-averaged field results from 0–5 Ma lavas from Kenya and the latitudinal variation of angular dispersion. *Geochemistry, Geophysics, Geosystems*, *11*, Q05005. https://doi.org/10.1029/2009GC002863

Opdyke, N. D., & Musgrave, R. (2004). Paleomagnetic results from the Newer Volcanics of Victoria: Contribution to the Time Averaged Field Initiative. *Geochemistry, Geophysics, Geosystems*, *5*, Q03H09. https://doi.org/10.1029/2003GC000632

Otake, H., Tanaka, H., Kono, M., & Saito, K. (1993). Paleomagnetic study of Pleistocene lavas and dikes of the Zao volcano group, Japan. *Journal of Geomagnetism and Geoelectricity*, *45*(7), 595–612. https://doi.org/10.5636/jgg.45.595

Panaiotu, C. G., Jicha, B. R., Singer, B. S., Ţugui, A., Seghedi, I., Panaiotu, A. G., et al. (2013). $^{40}Ar/^{39}Ar$ chronology and paleomagnetism of Quaternary basaltic lavas from the Persani Mountains (East Carpathians). *Physics of the Earth and Planetary Interiors*, *221*, 1–14. https://doi.org/10.1016/j.pepi.2013.06.007

Panaiotu, C. G., Vişan, M., Ţugui, A., Seghedi, I., & Panaiotu, A. G. (2012). Palaeomagnetism of the South Hargita volcanic rocks of the East Carpathians: Implications for tectonic rotations and palaeosecular variation in the past 5 Ma. *Geophysical Journal International*, *189*(1), 369–382. https://doi.org/10.1111/j.1365-246X.2012.05394.x

Panovska, S., & Constable, C. G. (2017). An activity index for geomagnetic paleosecular variation, excursions, and reversals. *Geochemistry Geophysics Geosystems*, *18*, 1366–1375. https://doi.org/10.1002/2016GC006668

Peña, R. M., Goguitchaichvili, A., Guilbaud, M.-N., Ruiz Martínez, V. C., Calvo Rathert, M., Siebe, C., et al. (2014). Paleomagnetic secular variation study of Ar-Ar dated lava flows from Tacambaro area (Central Mexico): Possible evidence of intra-Jaramillo geomagnetic excursion in volcanic rocks. *Physics of the Earth and Planetary Interiors*, *229*, 98–109. https://doi.org/10.1016/j.pepi.2014.01.005

Peña, R. M., Goguitchaichvili, A., Henry, B., Sanchez-Bettucci, L., Morales, J., Reyes, B., et al. (2011). Plio-Pleistocene paleomagnetic record from the Michoacan-Guanajuato monogenetic volcanic field (Western Mexico). *Studia Geophysica et Geodaetica*, *55*(2), 311–328. https://doi.org/10.1007/s11200-011-0017-2

Petronille, M., Goguitchaichvili, A., Henry, B., Alva-Valdivia, L. M., Rosas-Elguera, J., Urrutia-Fucugauchi, J., et al. (2005). Paleomagnetism of Ar-Ar dated lava flows from the Ceboruco-San Pedro volcanic field (Western Mexico): Evidence for the Matuyama-Brunhes transition precursor and a fully reversed geomagnetic event in the Brunhes Chron. *Journal of Geophysical Research*, *110*, B08101. https://doi.org/10.1029/2004JB003321

Quidelleur, X., Carlut, J., Tchilinguirian, P., Germa, A., & Gillot, P. Y. (2009). Paleomagnetic directions from mid-latitude sites in the Southern Hemisphere (Argentina): Contribution to time averaged field models. *Physics of the Earth and Planetary Interiors*, *172*(3–4), 199–209. https://doi.org/10.1016/j.pepi.2008.09.012

Quidelleur, X., & Courtillot, V. (1996). On low-degree spherical harmonic models of paleosecular variation. *Physics of the Earth and Planetary Interiors*, *95*(1–2), 55–77. https://doi.org/10.1016/0031-9201(95)03115-4

Quidelleur, X., Valet, J.-P., Courtillot, V., & Hulot, G. (1994). Long-term geometry of the geomagnetic field for the last five million years: An updated secular variation database. *Geophysical Research Letters*, *21*(15), 1639–1642. https://doi.org/10.1029/94GL01105

Rais, A., Laj, C., Surmont, J., Gillot, P. J., & Guillou, H. (1996). Geomagnetic field intensity between 70 000 and 130 000 years BP from a volcanic sequence on La Reunion, Indian Ocean. *Earth and Planetary Science Letters*, *140*(1–4), 173–189. https://doi.org/10.1016/0012-821X(96)00024-6

Riisager, J., Perrin, R., Riisager, P., & Ruffet, G. (2000). Paleomagnetism, paleointensity and geochronology of Miocene basalts and baked sediments from Velay Oriental, French Massif Central. *Journal of Geophysical Research*, *105*(B1), 883–896. https://doi.org/10.1029/1999JB900337

Roperch, P., Chauvin, A., Lara, L. E., & Moreno, H. (2015). Secular variation of the Earth's magnetic field and application to paleomagnetic dating of historical lava flows in Chile. *Physics of the Earth and Planetary Interiors*, *242*, 65–78. https://doi.org/10.1016/j.pepi.2015.03.005

Ruiz-Martinez, V. C., Urrutia-Fucugauchi, J., & Osete, M. L. (2010). Palaeomagnetism of the western and central sectors of the trans-Mexican volcanic belt—Implications for tectonic rotations and palaeosecular variation in the past 11 Ma. *Geophysical Journal International*, *180*(2), 577–595. https://doi.org/10.1111/j.1365-246X.2009.04447.x

Salis, J.-S., Bonhommet, N., & Levi, S. (1989). Paleointensity of the geomagnetic field from dated lavas of the Chaine des Puys, France 1.7–12 thousand years before present. *Journal of Geophysical Research*, *94*(B11), 15771–15784. https://doi.org/10.1029/JB094iB11p15771

Sánchez-Duque, A., Mejia, V., Opdyke, N. D., Huang, K., & Rosales-Rivera, A. (2016). Plio-Pleistocene paleomagnetic secular variation and time-averaged field: Ruiz-Tolima volcanic chain, Colombia. *Geochemistry Geophysics Geosystems*, *17*, 538–549. https://doi.org/10.1002/2015GC006149

Sbarbori, E., Tauxe, L., Goguitchaichvili, A., Urrutia-Fucugauchi, J., & Bohrson, W. A. (2009). Paleomagnetic behavior of volcanic rocks from Isla Socorro, Mexico. *Earth, Planets and Space*, *61*(1), 191–204. https://doi.org/10.1186/BF03352899

Stone, D. B., & Layer, P. W. (2006). Paleosecular variation and GAD studies of 0–2 Ma flow sequences from the Aleutian Islands, Alaska. *Geochemistry, Geophysics, Geosystems*, *7*, Q04H22. https://doi.org/10.1029/2005GC001007

Suttie, N., Biggin, A., & Holme, R. (2015). Robust estimators of palaeosecular variation. *Geophysical Journal International*, *200*(2), 1046–1051. https://doi.org/10.1093/gji/ggu443

Tanaka, H., Kamizaki, R., & Yamamoto, Y. (2007). Palaeomagnetism of the older Ontake volcano, Japan: Contributions to the palaeosecular variation for 750–400 ka, the lower half of the Brunhes Chron. *Geophysical Journal International*, *169*(1), 81–90. https://doi.org/10.1111/j.1365-246X.2006.03306.x

Tanaka, H., Kawamura, K., Nagao, K., & Houghton, B. (1997). K-Ar ages and paleosecular variation of direction and intensity from Quaternary lava sequences in the Ruapehu volcano, New Zealand. *Journal of Geomagnetism and Geoelectricity*, *49*(4), 587–599. https://doi.org/10.5636/jgg.49.587

Tanaka, H., & Kobayashi, T. (2003). Paleomagnetism of the Late Quaternary Ontake volcano, Japan: Directions, intensities, and excursions. *Earth, Planets and Space*, *55*(4), 189–202. https://doi.org/10.1186/BF03351748

Tanaka, H., Komuro, N., & Turner, G. M. (2009). Palaeosecular variation for 0.1–21 ka from Okataina Volcanic Centre, New Zealand. *Earth, Planets and Space*, *61*(1), 213–225. https://doi.org/10.1186/BF03352901

Tanty, C., Carlut, J., Valet, J.-P., & Germa, A. (2015). Palaeosecular variation recorded by 9 ka to 2.5 Ma old lavas from Martinique Island: New evidence for the La Palma aborted reversal ~617 ka ago. *Geophysical Journal International*, *200*(2), 9150932. https://doi.org/10.1093/gji/ggu423

Tauxe, L., Constable, C. G., Johnson, C. L., Koppers, A. A. P., Miller, W., & Staudigel, H. (2003). Paleomagnetism of the southwestern U.S.A. recorded by 0–5 Ma igneous rocks. *Geochemistry Geophysics Geosystems*, *4*(4), 8802. https://doi.org/10.1029/2002GC000343

Tauxe, L., Gans, P. B., & Mankinen, E. A. (2004). Paleomagnetism and $^{40}Ar/^{39}Ar$ ages from volcanics extruded during the Matuyama and Brunhes Chrons near McMurdo Sound, Antarctica. *Geochemistry Geophysics Geosystems*, *5*, Q06H12. https://doi.org/10.1029/2003GC000656

Tauxe, L., & Kent, D. V. (2004). A simplified statistical model for the geomagnetic field and the detection of shallow bias in paleomagnetic inclinations: Was the ancient magnetic field dipolar? In J. E. T. Channell, D. V. Kent, W. Lowrie, & J. G. Meert (Eds.), *Timescales of the paleomagnetic field* (Vol. 145, pp. 101–116). Washington, DC: American Geophysical Union.

Tauxe, L., Luskin, C., Selkin, P., Gans, P. B., & Calvert, A. (2004). Paleomagnetic results from the Snake River Plain: Contribution to the time-averaged field global database. *Geochemistry, Geophysics, Geosystems*, *5*, Q08H13. https://doi.org/10.1029/2003GC000661

Tauxe, L., Shaar, R., Jonestrask, L., Swanson-Hysell, N. L., Minnett, R., Koppers, A. A. P., et al. (2016). PmagPy: Software package for paleomagnetic data analysis and a bridge to the Magnetics Information Consortium (MagIC) database. *Geochemistry, Geophysics, Geosystems*, *17*, 2450–2463. https://doi.org/10.1002/2016GC006307

Tauxe, L., Staudigel, H., & Wijbrans, J. R. (2000). Paleomagnetism and $^{40}Ar/^{39}Ar$ ages from La Palma in the Canary Islands. *Geochemistry, Geophysics, Geosystems*, *1*(9), 2000GC000063. https://doi.org/10.1029/2000GC000063

Udagawa, S., Kitagawa, H., Gudmundsson, A., Hiroi, O., Koyaguchi, T., Tanaka, H., et al. (1999). Age and magnetism of lavas in Jökuldalur area, Eastern Iceland: Gilsá event revisited. *Physics of the Earth and Planetary Interiors*, *115*(2), 147–171. https://doi.org/10.1016/S0031-9201(99)00073-4

Valet, J. P., Meynadier, L., & Guyodo, Y. (2005). Geomagnetic dipole strength and reversal rate over the past two million years. *Nature*, *435*(7043), 802–805. https://doi.org/10.1038/nature03674

Valet, J. P., Tric, E., Herrero-Bervera, E., Meynadier, L., & Lockwood, J. P. (1998). Absolute paleointensity from Hawaiian lavas younger than 35 ka. *Earth and Planetary Science Letters*, *161*(1–4), 19–32. https://doi.org/10.1016/S0012-821X(98)00133-2

Vandamme, D. (1994). A new method to determine paleosecular variation. *Physics of the Earth and Planetary Interiors*, *85*(1–2), 131–142. https://doi.org/10.1016/0031-9201(94)90012-4

Yamamoto, Y., Shimura, K., Tsunakawa, H., Kogiso, T., Uto, K., Barsczus, H., et al. (2002). Geomagnetic paleosecular variation for the past 5 Ma in the Society Islands, French Polynesia. *Earth, Planets and Space*, *54*(7), 797–802. https://doi.org/10.1186/BF03351733

Yamamoto, Y., Tsunakawa, H., Shaw, J., & Kono, M. (2007). Paleomagnetism of the Datong Monogenetic volcanoes in China: Paleodirection and paleointensity during the middle to early Brunhes Chron. *Earth, Planets and Space*, *59*(7), 727–746. https://doi.org/10.1186/BF03352736

Ziegler, L. B., Constable, C. G., Johnson, C. L., & Tauxe, L. (2011). PADM2M: A penalized maximum likelihood model of the 0–2 Ma palaeomagnetic axial dipole moment. *Geophysical Journal International*, *184*, 1069–1089. https://doi.org/10.1111/j.1365-246X.2010.04905.x